International Tables for Crystallography (2006). Vol. B, Chapter 5.1, pp. 534–551.

5.1. Dynamical theory of X-ray diffraction

BY A. AUTHIER

5.1.1. Introduction

The first experiment on X-ray diffraction by a crystal was performed by W. Friedrich, P. Knipping and M. von Laue in 1912 and Bragg's law was derived in 1913 (Bragg, 1913). Geometrical and dynamical theories for the intensities of the diffracted X-rays were developed by Darwin (1914*a*,*b*). His dynamical theory took into account the interaction of X-rays with matter by solving recurrence equations that describe the balance of partially transmitted and partially reflected amplitudes at each lattice plane. This is the first form of the dynamical theory of X-ray diffraction. It gives correct expressions for the reflected intensities and was extended to the absorbing-crystal case by Prins (1930). A second form of dynamical theory was introduced by Ewald (1917) as a continuation of his previous work on the diffraction of optical waves by crystals. He took into account the interaction of X-rays with matter by considering the crystal to be a periodic distribution of dipoles which were excited by the incident wave. This theory also gives the correct expressions for the reflected and transmitted intensities, and it introduces the fundamental notion of a wavefield, which is necessary to understand the propagation of X-rays in perfect or deformed crystals. Ewald's theory was later modified by von Laue (1931), who showed that the interaction could be described by solving Maxwell's equations in a medium with a continuous, triply periodic distribution of dielectric susceptibility. It is this form which is most widely used today and which will be presented in this chapter.

The geometrical (or kinematical) theory, on the other hand, considers that each photon is scattered only once and that the interaction of X-rays with matter is so small it can be neglected. It can therefore be assumed that the amplitude incident on every diffraction centre inside the crystal is the same. The total diffracted amplitude is then simply obtained by adding the individual amplitudes diffracted by each diffracting centre, taking into account only the geometrical phase differences between them and neglecting the interaction of the radiation with matter. The result is that the distribution of diffracted amplitudes in reciprocal space is the Fourier transform of the distribution of diffracting centres in physical space. Following von Laue (1960), the expression *geometrical theory* will be used throughout this chapter when referring to these geometrical phase differences.

The first experimentally measured reflected intensities were not in agreement with the theoretical values obtained with the more rigorous dynamical theory, but rather with the simpler geometrical theory. The integrated reflected intensities calculated using geometrical theory are proportional to the square of the structure factor, while the corresponding expressions calculated using dynamical theory for an infinite perfect crystal are proportional to the modulus of the structure factor. The integrated intensity calculated by geometrical theory is also proportional to the volume of the crystal bathed in the incident beam. This is due to the fact that one neglects the decrease of the incident amplitude as it progresses through the crystal and a fraction of it is scattered away. According to geometrical theory, the diffracted intensity would therefore increase to infinity if the volume of the crystal was increased to infinity, which is of course absurd. The theory only works because the strength of the interaction is very weak and if it is applied to very small crystals. How small will be shown quantitatively in Sections 5.1.6.5 and 5.1.7.2. Darwin (1922) showed that it can also be applied to large imperfect crystals. This is done using the model of mosaic crystals (Bragg *et al*., 1926). For perfect or nearly perfect crystals, dynamical theory should be used. Geometrical theory presents another drawback: it gives no indication as to the phase of the reflected wave. This is due to the fact that it is based on the Fourier transform of the electron density limited by the external shape of the crystal. This is not important when one is only interested in measuring the reflected intensities. For any problem where the phase is important, as is the case for multiple reflections, interference between coherent blocks, standing waves *etc.*, dynamical theory should be used, even for thin or imperfect crystals.

Until the 1940s, the applications of dynamical theory were essentially intensity measurements. From the 1950s to the 1970s, applications were related to the properties (absorption, interference, propagation) of wavefields in perfect or nearly perfect crystals: anomalous transmission, diffraction of spherical waves, interpretation of images on X-ray topographs, accurate measurement of form factors, lattice-parameter mapping. In recent years, they have been concerned mainly with crystal optics, focusing and the design of monochromators for synchrotron radiation [see, for instance, Batterman & Bilderback (1991)], the location of atoms at crystal surfaces and interfaces using the standing-waves method [see, for instance, the reviews by Authier (1989) and Zegenhagen (1993)], attempts to determine phases using multiple reflections [see, for instance, Chang (1987) and Hümmer & Weckert (1995)], characterization of the crystal perfection of epilayers and superlattices by high-resolution diffractometry [see, for instance, Tanner (1990) and Fewster (1993)], *etc.*

For reviews of dynamical theory, see Zachariasen (1945), von Laue (1960), James (1963), Batterman & Cole (1964), Authier (1970), Kato (1974), Brümmer & Stephanik (1976), Pinsker (1978), Authier & Malgrange (1998), and Authier (2001). Topography is described in Chapter 2.7 of *IT* C (1999), in Tanner (1976) and in Tanner & Bowen (1992). For the use of Bragg-angle measurements for accurate lattice-parameter mapping, see Hart (1981).

A reminder of some basic concepts in electrodynamics is given in Section A5.1.1.1 of the Appendix.

5.1.2. Fundamentals of plane-wave dynamical theory

5.1.2.1. *Propagation equation*

The wavefunction Ψ associated with an electron or a neutron beam is *scalar* while an electromagnetic wave is a *vector* wave. When propagating in a medium, these waves are solutions of a *propagation equation*. For electrons and neutrons, this is Schrödinger's equation, which can be rewritten as

$$\Delta\Psi + 4\pi^2 k^2(1+\chi)\Psi = 0, \qquad (5.1.2.1)$$

where $k = 1/\lambda$ is the wavenumber in a vacuum, $\chi = \varphi/W$ (φ is the potential in the crystal and W is the accelerating voltage) in the case of electron diffraction and $\chi = -2mV(\mathbf{r})/h^2k^2$ [$V(\mathbf{r})$ is the Fermi pseudo-potential and h is Planck's constant] in the case of neutron diffraction. The dynamical theory of electron diffraction is treated in Chapter 5.2 [note that a different convention is used in Chapter 5.2 for the scalar wavenumber: $k = 2\pi/\lambda$; compare, for example, equation (5.2.2.1) and its equivalent, equation (5.1.2.1)] and the dynamical theory of neutron diffraction is treated in Chapter 5.3.

In the case of X-rays, the propagation equation is deduced from Maxwell's equations after neglecting the interaction with protons. Following von Laue (1931, 1960), it is assumed that the positive charge of the nuclei is distributed in such a way that the medium is everywhere locally neutral and that there is no current. As a first approximation, magnetic interaction, which is very weak, is not taken into account in this review. The propagation equation is

derived in Section A5.1.1.2 of the Appendix. Expressed in terms of the local electric displacement, $\mathbf{D}(\mathbf{r})$, it is given for monochromatic waves by

$$\Delta\mathbf{D}(\mathbf{r}) + \text{ curl curl } \chi\mathbf{D}(\mathbf{r}) + 4\pi^2k^2\mathbf{D}(\mathbf{r}) = 0. \qquad (5.1.2.2)$$

The interaction of X-rays with matter is characterized in equation (5.1.2.2) by the parameter χ, which is the dielectric susceptibility. It is classically related to the electron density $\rho(\mathbf{r})$ by

$$\chi(\mathbf{r}) = -R\lambda^2\rho(\mathbf{r})/\pi, \qquad (5.1.2.3)$$

where $R = 2.81794 \times 10^{-6}$ nm is the classical radius of the electron [see equation (A5.1.1.2) in Section A5.1.1.2 of the Appendix].

The dielectric susceptibility, being proportional to the electron density, is triply periodic in a crystal. It can therefore be expanded in Fourier series:

$$\chi = \sum_{\mathbf{h}} \chi_h \exp(2\pi i\mathbf{h}\cdot\mathbf{r}), \qquad (5.1.2.4)$$

where $\mathbf{h}$ is a reciprocal-lattice vector and the summation is extended over all reciprocal-lattice vectors. The sign convention adopted here for Fourier expansions of periodic functions is the *standard crystallographic* sign convention defined in Section 2.5.2.3. The relative orientations of wavevectors and reciprocal-lattice vectors are defined in Fig. 5.1.2.1, which represents schematically a Bragg reflection in direct and reciprocal space (Figs. 5.1.2.1*a* and 5.1.2.1*b*, respectively).

The coefficients χ_h of the Fourier expansion of the dielectric susceptibility are related to the usual structure factor F_h by

$$\chi_h = -R\lambda^2F_h/(\pi V), \qquad (5.1.2.5)$$

where V is the volume of the unit cell and the structure factor is given by

$$\begin{aligned} F_h &= \sum_j (f_j + f_j' + if_j'') \exp(-M_j - 2\pi i\mathbf{h}\cdot\mathbf{r}_j) \\ &= |F_h| \exp(i\varphi_h). \end{aligned} \qquad (5.1.2.6)$$

f_j is the form factor of atom j, f_j' and f_j'' are the dispersion corrections [see, for instance, *IT* C, Section 4.2.6] and $\exp(-M_j)$ is the Debye–Waller factor. The summation is over all the atoms in the unit cell. The phase φ_h of the structure factor depends of course on the choice of origin of the unit cell. The Fourier coefficients χ_h are dimensionless. Their order of magnitude varies from 10^{-5} to 10^{-7} depending on the wavelength and the structure factor. For example, χ_h is -9.24×10^{-6} for the 220 reflection of silicon for Cu $K\alpha$ radiation.

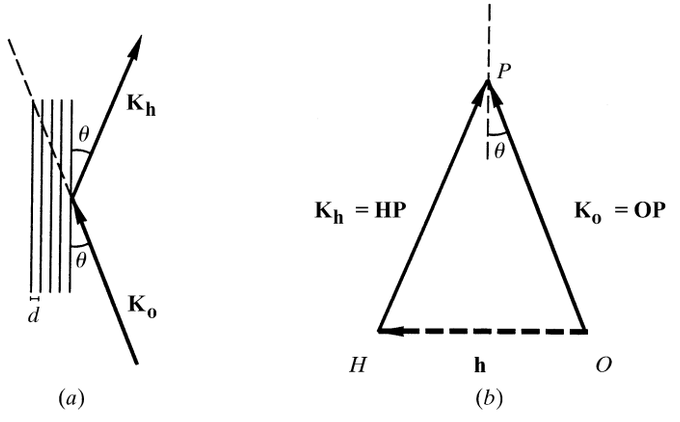

Fig. 5.1.2.1. Bragg reflection. (*a*) Direct space. Bragg reflection of a wave of wavevector $\mathbf{K_o}$ incident on a set of lattice planes of spacing d. The reflected wavevector is $\mathbf{K_h}$. Bragg's law $2d\sin\theta = n\lambda$ can also be written $2d_{hkl}\sin\theta = \lambda$, where $d_{hkl} = d/n = 1/OH = 1/h$ is the inverse of the length of the corresponding reciprocal-lattice vector $\mathbf{OH} = \mathbf{h}$ (see part *b*). (*b*) Reciprocal space. P is the tie point of the wavefield consisting of the incident wave $\mathbf{K_o} = \mathbf{OP}$ and the reflected wave $\mathbf{K_h} = \mathbf{HP}$. Note that the wavevectors are oriented *towards* the tie point.

In an absorbing crystal, absorption is taken into account phenomenologically through the imaginary parts of the index of refraction and of the wavevectors. The dielectric susceptibility is written

$$\chi = \chi_r + i\chi_i. \qquad (5.1.2.7)$$

The real and imaginary parts of the susceptibility are triply periodic in a crystalline medium and can be expanded in a Fourier series,

$$\begin{aligned} \chi_r &= \sum_{\mathbf{h}} \chi_{rh} \exp(2\pi i\mathbf{h}\cdot\mathbf{r}) \\ \chi_i &= \sum_{\mathbf{h}} \chi_{ih} \exp(2\pi i\mathbf{h}\cdot\mathbf{r}), \end{aligned} \qquad (5.1.2.8)$$

where

$$\begin{aligned} \chi_{rh} &= -R\lambda^2F_{rh}/(\pi V), \\ \chi_{ih} &= -R\lambda^2F_{ih}/(\pi V) \end{aligned} \qquad (5.1.2.9)$$

and

$$\begin{aligned} F_{rh} &= \sum_j (f_j + f_j') \exp(-M_j - 2\pi i\mathbf{h}\cdot\mathbf{r}_j) \\ &= |F_{rh}| \exp(i\varphi_{rh}), \qquad (5.1.2.10a) \\ F_{ih} &= \sum_j (f_j'') \exp(-M_j - 2\pi i\mathbf{h}\cdot\mathbf{r}_j) \\ &= |F_{ih}| \exp(i\varphi_{ih}). \qquad (5.1.2.10b) \end{aligned}$$

It is important to note that

$$F_{rh}^* = F_{r\bar{h}} \text{ and } F_{ih}^* = F_{i\bar{h}} \text{ but that } F_h^* \neq F_{\bar{h}}, \qquad (5.1.2.11)$$

where f^* is the imaginary conjugate of f.

The *index of refraction* of the medium for X-rays is

$$n = 1 + \chi_{ro}/2 = 1 - R\lambda^2F_o/(2\pi V), \qquad (5.1.2.12)$$

where F_o/V is the number of electrons per unit volume. This index is very slightly smaller than one. It is for this reason that specular reflection of X-rays takes place at grazing angles. From the value of the critical angle, $(-\chi_{ro})^{1/2}$, the electron density F_o/V of a material can be determined.

The linear absorption coefficient is

$$\mu_o = -2\pi k\chi_{io} = 2R\lambda F_{io}/V. \qquad (5.1.2.13)$$

For example, it is 143.2 cm^{-1} for silicon and Cu $K\alpha$ radiation.

5.1.2.2. *Wavefields*

The notion of a wavefield, introduced by Ewald (1917), is one of the most fundamental concepts in dynamical theory. It results from the fact that since the propagation equation (5.1.2.2) is a second-order partial differential equation with a periodic interaction coefficient, its solution has the same periodicity,

$$\mathbf{D} = \exp(-2\pi i\mathbf{K_o}\cdot\mathbf{r}) \sum_{\mathbf{h}} \mathbf{D_h} \exp(2\pi i\mathbf{h}\cdot\mathbf{r}), \qquad (5.1.2.14)$$

where the summation is over all reciprocal-lattice vectors $\mathbf{h}$. Equation (5.1.2.14) can also be written

$$\mathbf{D} = \sum_{\mathbf{h}} \mathbf{D_h} \exp(-2\pi i\mathbf{K_h}\cdot\mathbf{r}), \qquad (5.1.2.15)$$

where

$$\mathbf{K_h} = \mathbf{K_o} - \mathbf{h}. \qquad (5.1.2.16)$$

Expression (5.1.2.15) shows that the solution of the propagation equation can be interpreted as an infinite sum of plane waves with amplitudes $\mathbf{D_h}$ and wavevectors $\mathbf{K_h}$. This sum is a *wavefield*, or *Ewald wave*. The same expression is used to describe the propagation of any wave in a periodic medium, such as phonons or electrons in a solid. Expression (5.1.2.14) was later called a *Bloch wave* by solid-state physicists.

The wavevectors in a wavefield are deduced from one another by translations of the reciprocal lattice [expression (5.1.2.16)]. They can be represented geometrically as shown in Fig. 5.1.2.1(*b*). The wavevectors $\mathbf{K_o} = \mathbf{OP}$; $\mathbf{K_h} = \mathbf{HP}$ are drawn *away* from reciprocal-lattice points. Their common extremity, *P*, called the *tie point* by Ewald, characterizes the wavefield.

In an absorbing crystal, wavevectors have an imaginary part,

$$\mathbf{K_o} = \mathbf{K}_{or} + i\mathbf{K}_{oi};\ \ \mathbf{K_h} = \mathbf{K}_{hr} + i\mathbf{K}_{hi},$$

and (5.1.2.16) shows that all wavevectors have the same imaginary part,

$$\mathbf{K}_{oi} = \mathbf{K}_{hi}, \qquad (5.1.2.17)$$

and therefore undergo the same absorption. This is one of the most important properties of wavefields.

5.1.2.3. *Boundary conditions at the entrance surface*

The choice of the '**o**' component of expansion (5.1.2.15) is arbitrary in an infinite medium. In a semi-infinite medium where the waves are created at the interface with a vacuum or air by an incident plane wave with wavevector $\mathbf{K}_\mathbf{o}^{(a)}$ (using von Laue's notation), the choice of $\mathbf{K_o}$ is determined by the boundary conditions.

This condition for wavevectors at an interface demands that their tangential components should be continuous across the boundary, in agreement with Descartes–Snell's law. This condition is satisfied when the difference between the wavevectors on each side of the interface is parallel to the normal to the interface. This is shown geometrically in Fig. 5.1.2.2 and formally in (5.1.2.18):

$$\mathbf{K_o} - \mathbf{K}_\mathbf{o}^{(a)} = \mathbf{OP} - \mathbf{OM} = \overline{MP} \cdot \mathbf{n}, \qquad (5.1.2.18)$$

where $\mathbf{n}$ is a unit vector normal to the crystal surface, oriented towards the inside of the crystal.

There is no absorption in a vacuum and the incident wavevector $\mathbf{K}_\mathbf{o}^{(a)}$ is real. Equation (5.1.2.18) shows that it is the component normal to the interface of wavevector $\mathbf{K_o}$ which has an imaginary part,

$$\mathbf{K}_{oi} = \mathcal{I}(\overline{MP}) \cdot \mathbf{n} = -\mu\mathbf{n}/(4\pi\gamma_o), \qquad (5.1.2.19)$$

where $\mathcal{I}(f)$ is the imaginary part of f, $\gamma_o = \cos(\mathbf{n} \cdot \mathbf{s_o})$ and $\mathbf{s_o}$ is a unit vector in the incident direction. When there is more than one wave in the wavefield, the effective absorption coefficient μ can differ significantly from the normal value, μ_o, given by (5.1.2.13) – see Section 5.1.5.

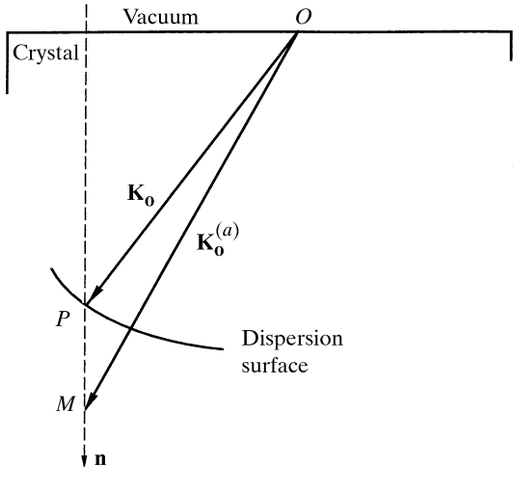

Fig. 5.1.2.2. Boundary condition for wavevectors at the entrance surface of the crystal.

5.1.2.4. *Fundamental equations of dynamical theory*

In order to obtain the solution of dynamical theory, one inserts expansions (5.1.2.15) and (5.1.2.4) into the propagation equation (5.1.2.2). This leads to an equation with an infinite sum of terms. It is shown to be equivalent to an infinite system of linear equations which are the *fundamental equations* of dynamical theory. Only those terms in (5.1.2.15) whose wavevector magnitudes K_h are very close to the vacuum value, k, have a non-negligible amplitude. These wavevectors are associated with reciprocal-lattice points that lie very close to the Ewald sphere. Far from any Bragg reflection, their number is equal to 1 and a single plane wave propagates through the medium. In general, for X-rays, there are only two reciprocal-lattice points on the Ewald sphere. This is the so-called *two-beam* case to which this treatment is limited. There are, however, many instances where several reciprocal-lattice points lie simultaneously on the Ewald sphere. This corresponds to the *many-beam* case which has interesting applications for the determination of phases of reflections [see, for instance, Chang (1987) and Hümmer & Weckert (1995)]. On the other hand, for electrons, there are in general many reciprocal-lattice points close to the Ewald sphere and many wavefields are excited simultaneously (see Chapter 5.2).

In the two-beam case, for reflections that are not highly asymmetric and for Bragg angles that are not close to $\pi/2$, the fundamental equations of dynamical theory reduce to

$$\begin{aligned} 2X_oD_o - kC\chi_{\bar{h}}D_h &= 0 \\ -kC\chi_hD_o + 2X_hD_h &= 0, \end{aligned} \qquad (5.1.2.20)$$

where $C = 1$ if $\mathbf{D_h}$ is normal to the $\mathbf{K_o}, \mathbf{K_h}$ plane and $C = \cos 2\theta$ if $\mathbf{D_h}$ lies in the plane; this is due to the fact that the amplitude with which electromagnetic radiation is scattered is proportional to the sine of the angle between the direction of the electric vector of the incident radiation and the direction of scattering (see, for instance, *IT* C, Section 6.2.2). The polarization of an electromagnetic wave is classically related to the orientation of the electric vector; in dynamical theory it is that of the electric displacement which is considered (see Section A5.1.1.3 of the Appendix).

The system (5.1.2.20) is therefore a system of four equations which admits four solutions, two for each direction of polarization. In the *non-absorbing* case, to a very good approximation,

$$\begin{aligned} X_o &= K_o - nk, \\ X_h &= K_h - nk. \end{aligned} \qquad (5.1.2.21)$$

In the case of an *absorbing crystal*, X_o and K_h are complex. Equation (5.1.5.2) gives the full expression for X_o.

5.1.2.5. *Dispersion surface*

The fundamental equations (5.1.2.20) of dynamical theory are a set of linear homogeneous equations whose unknowns are the amplitudes of the various waves which make up a wavefield. For the solution to be non-trivial, the determinant of the set must be set equal to zero. This provides a secular equation relating the magnitudes of the wavevectors of a given wavefield. This equation is that of the locus of the tie points of all the wavefields that may

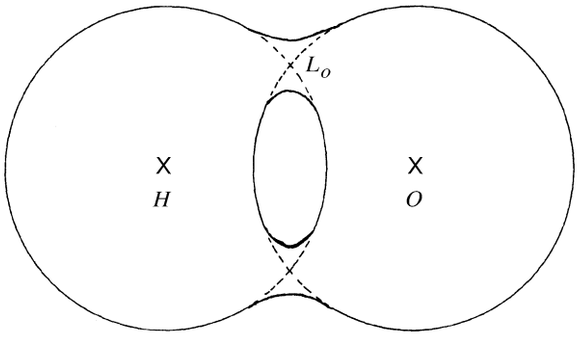

Fig. 5.1.2.3. Intersection of the dispersion surface with the plane of incidence. The dispersion surface is a connecting surface between the two spheres centred at reciprocal-lattice points O and H and with radius nk. L_o is the Lorentz point.

propagate in the crystal with a given frequency. This locus is called the *dispersion surface*. It is a constant-energy surface and is the equivalent of the index surface in optics. It is the X-ray analogue of the constant-energy surfaces known as Fermi surfaces in the electron band theory of solids.

In the two-beam case, the dispersion surface is a surface of revolution around the diffraction vector **OH**. It is made from two spheres and a connecting surface between them. The two spheres are centred at O and H and have the same radius, nk. Fig. 5.1.2.3 shows the intersection of the dispersion surface with a plane passing through **OH**. When the tie point lies on one of the two spheres, far from their intersection, only one wavefield propagates inside the crystal. When it lies on the connecting surface, two waves are excited simultaneously. The equation of this surface is obtained by equating to zero the determinant of system (5.1.2.20):

$$X_o X_h = k^2 C^2 \chi_h \chi_{\bar{h}}/4. \qquad (5.1.2.22)$$

Equations (5.1.2.21) show that, in the zero-absorption case, X_o and X_h are to be interpreted as the distances of the tie point P from the spheres centred at O and H, respectively. From (5.1.2.20) it can be seen that they are of the order of the vacuum wavenumber times the Fourier coefficient of the dielectric susceptibility, that is five or six orders of magnitude smaller than k. The two spheres can therefore be replaced by their tangential planes. Equation (5.1.2.22) shows that the product of the distances of the tie point from these planes is constant. The intersection of the dispersion surface with the plane passing through **OH** is therefore a hyperbola (Fig. 5.1.2.4) whose diameter [using (5.1.2.5) and (5.1.2.22)] is

$$\overline{A_{o2}A_{o1}} = |C|R\lambda(F_h F_{\bar{h}})^{1/2}/(\pi V \cos\theta). \qquad (5.1.2.23)$$

It can be noted that the larger the diameter of the dispersion surface, the larger the structure factor, that is, the stronger the interaction of the waves with the matter. When the polarization is parallel to the plane of incidence ($C = \cos 2\theta$), the interaction is weaker.

The asymptotes T_o and T_h to the hyperbola are tangents to the circles centred at O and H, respectively. Their intersection, L_o, is called the *Lorentz point* (Fig. 5.1.2.4).

A wavefield propagating in the crystal is characterized by a tie point P on the dispersion surface and two waves with wavevectors $\mathbf{K_o} = \mathbf{OP}$ and $\mathbf{K_h} = \mathbf{HP}$, respectively. The ratio, ξ, of their amplitudes D_h and D_o is given by means of (5.1.2.20):

$$\xi = \frac{D_h}{D_o} = \frac{2X_o}{kC\chi_{\bar{h}}} = \frac{-2\pi V X_o}{R\lambda C F_{\bar{h}}}. \qquad (5.1.2.24)$$

The hyperbola has two branches, 1 and 2, for each direction of polarization, that is, for $C = 1$ or $\cos 2\theta$ (Fig. 5.1.2.5). Branch 2 is

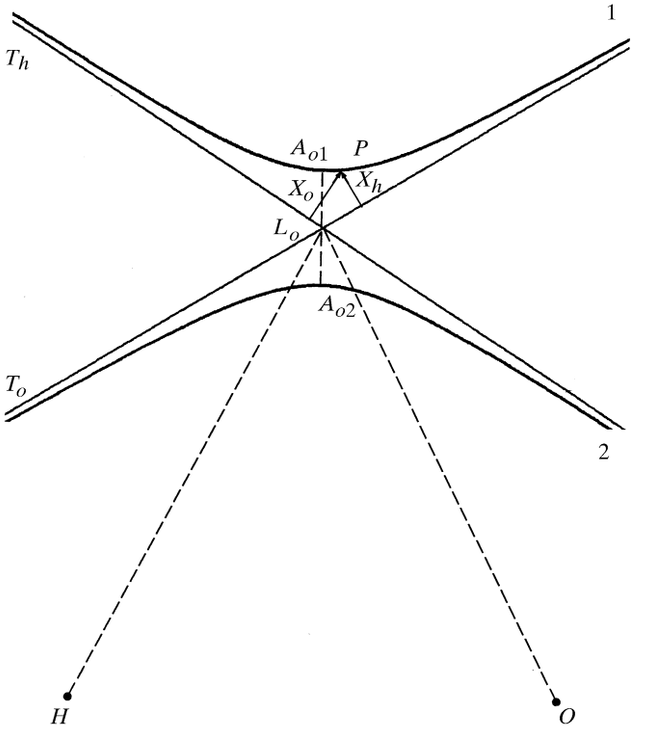

Fig. 5.1.2.4. Intersection of the dispersion surface with the plane of incidence shown in greater detail. The Lorentz point L_o is far away from the nodes O and H of the reciprocal lattice: $OL_o = HL_o = 1/\lambda$ is about 10^5 to 10^6 times larger than the diameter $A_{o1}A_{o2}$ of the dispersion surface.

the one situated on the same side of the asymptotes as the reciprocal-lattice points O and H. Given the orientation of the wavevectors, which has been chosen away from the reciprocal-lattice points (Fig. 5.1.2.1*b*), the coordinates of the tie point, X_o and X_h, are positive for branch 1 and negative for branch 2. The phase of ξ is therefore equal to $\pi + \varphi_h$ and to φ_h for the two branches, respectively, where φ_h is the phase of the structure factor [equation (5.1.2.6)]. This difference of π between the two branches has important consequences for the properties of the wavefields.

As mentioned above, owing to absorption, wavevectors are actually complex and so is the dispersion surface.

5.1.2.6. *Propagation direction*

The energy of all the waves in a given wavefield propagates in a common direction, which is obtained by calculating either the group velocity or the Poynting vector [see Section A5.1.1.4, equation (A5.1.1.8) of the Appendix]. It can be shown that, averaged over time and the unit cell, the Poynting vector of a wavefield is

$$\mathbf{S} = (c/\varepsilon_0)\exp(4\pi\mathbf{K_{oi}}\cdot\mathbf{r})\left[|D_o|^2\mathbf{s_o} + |D_h|^2\mathbf{s_h}\right], \qquad (5.1.2.25)$$

where $\mathbf{s_o}$ and $\mathbf{s_h}$ are unit vectors in the $\mathbf{K_o}$ and $\mathbf{K_h}$ directions, respectively, c is the velocity of light and ε_0 is the dielectric permittivity of a vacuum. This result was first shown by von Laue (1952) in the two-beam case and was generalized to the n-beam case by Kato (1958).

From (5.1.2.25) and equation (5.1.2.22) of the dispersion surface, it can be shown that the propagation direction of the wavefield lies along the normal to the dispersion surface at the tie point (Fig. 5.1.2.5). This result is also obtained by considering the group velocity of the wavefield (Ewald, 1958; Wagner, 1959). The angle α

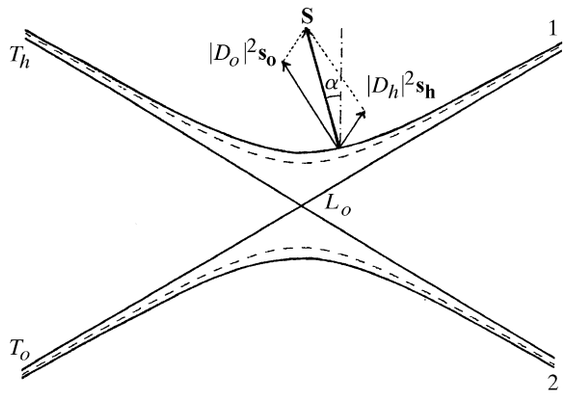

Fig. 5.1.2.5. Dispersion surface for the two states of polarization. Solid curve: polarization normal to the plane of incidence ($C = 1$); broken curve: polarization parallel to the plane of incidence ($C = \cos 2\theta$). The direction of propagation of the energy of the wavefields is along the Poynting vector, **S**, normal to the dispersion surface.

between the propagation direction and the lattice planes is given by

$$\tan\alpha = \left[(1 - |\xi|^2)/(1 + |\xi|^2)\right] \tan\theta. \qquad (5.1.2.26)$$

It should be noted that the propagation direction varies between $\mathbf{K_o}$ and $\mathbf{K_h}$ for both branches of the dispersion surface.

5.1.3. Solutions of plane-wave dynamical theory

5.1.3.1. *Departure from Bragg's law of the incident wave*

The wavefields excited in the crystal by the incident wave are determined by applying the boundary condition mentioned above for the continuity of the tangential component of the wavevectors (Section 5.1.2.3). Waves propagating in a vacuum have wavenumber $k = 1/\lambda$. Depending on whether they propagate in the incident or in the reflected direction, the common extremity, M, of their wavevectors

$$\mathbf{OM} = \mathbf{K_o^{(a)}} \text{ and } \mathbf{HM} = \mathbf{K_h^{(a)}}$$

lies on spheres of radius k and centred at O and H, respectively. The intersections of these spheres with the plane of incidence are two circles which can be approximated by their tangents T_o' and T_h' at their intersection point, L_a, or *Laue point* (Fig. 5.1.3.1).

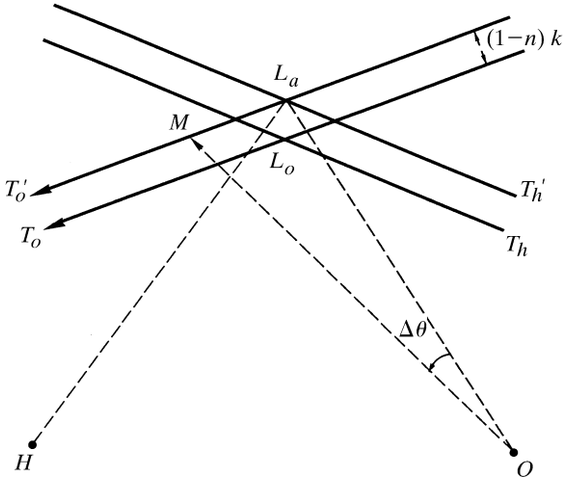

Fig. 5.1.3.1. Departure from Bragg's law of an incident wave.

Bragg's condition is exactly satisfied according to the geometrical theory of diffraction when M lies at L_a. The departure $\Delta\theta$ from Bragg's incidence of an incident wave is defined as the angle between the corresponding wavevectors **OM** and $\mathbf{OL}_a$. As $\Delta\theta$ is very small compared to the Bragg angle in the general case of X-rays or neutrons, one may write

$$\begin{aligned} \mathbf{K_o^{(a)}} &= \mathbf{OM} = \mathbf{OL}_a + \mathbf{L}_a\mathbf{M}, \\ \Delta\theta &= \overline{L_aM}/k. \end{aligned} \qquad (5.1.3.1)$$

The tangent T_o' is oriented in such a way that $\Delta\theta$ is negative when the angle of incidence is smaller than the Bragg angle.

5.1.3.2. *Transmission and reflection geometries*

The boundary condition for the continuity of the tangential component of the wavevectors is applied by drawing from M a line, **Mz**, parallel to the normal **n** to the crystal surface. The tie points of the wavefields excited in the crystal by the incident wave are at the intersections of this line with the dispersion surface. Two different situations may occur:

(*a*) *Transmission, or Laue case* (Fig. 5.1.3.2). The normal to the crystal surface drawn from M intersects *both* branches of the dispersion surface (Fig. 5.1.3.2*a*). The reflected wave is then directed towards the *inside* of the crystal (Fig. 5.1.3.2*b*). Let γ_o and γ_h be the cosines of the angles between the normal to the crystal surface, **n**, and the incident and reflected directions, respectively:

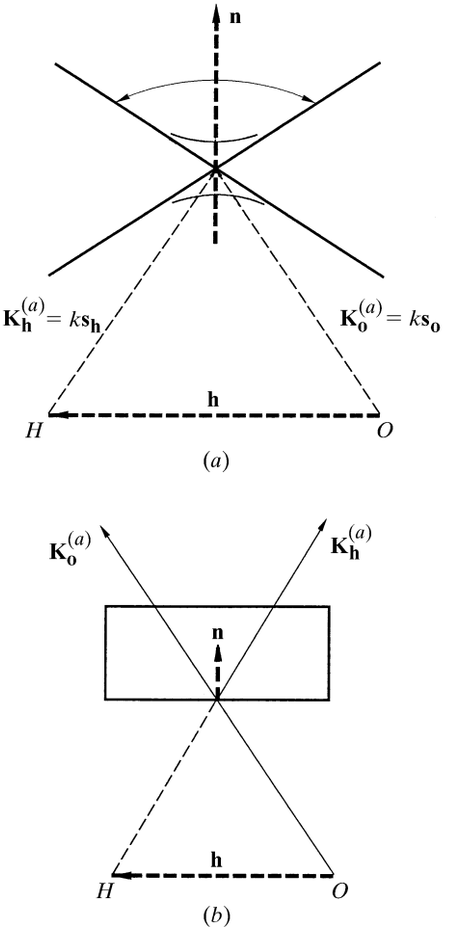

Fig. 5.1.3.2. Transmission, or Laue, geometry. (*a*) Reciprocal space; (*b*) direct space.

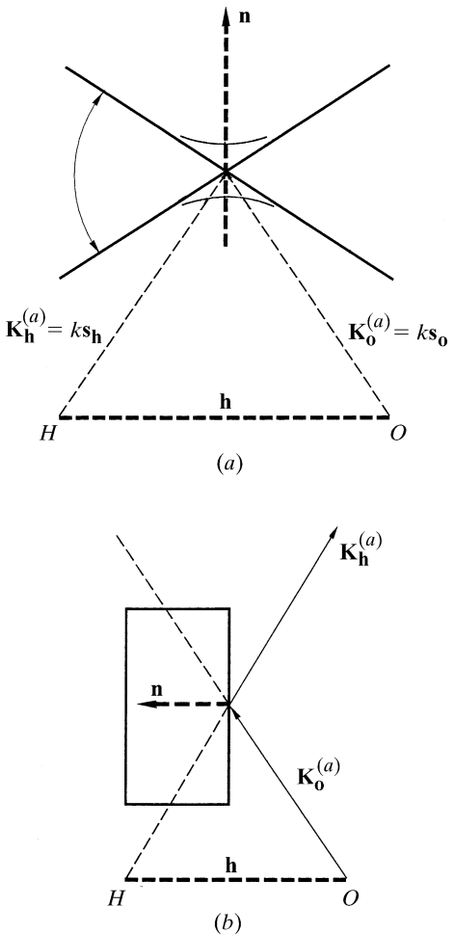

Fig. 5.1.3.3. Reflection, or Bragg, geometry. (*a*) Reciprocal space; (*b*) direct space.

$$\gamma_o = \cos(\mathbf{n}, \mathbf{s_o}); \quad \gamma_h = \cos(\mathbf{n}, \mathbf{s_h}). \tag{5.1.3.2}$$

It will be noted that they are both positive, as is their ratio,

$$\gamma = \gamma_h/\gamma_o. \tag{5.1.3.3}$$

This is the *asymmetry ratio*, which is very important since the width of the rocking curve is proportional to its square root [equation (5.1.3.6)].

(*b*) *Reflection, or Bragg case* (Fig. 5.1.3.3). In this case there are three possible situations: the normal to the crystal surface drawn from *M* intersects either branch 1 or branch 2 of the dispersion surface, or the intersection points are imaginary (Fig. 5.1.3.3*a*). The reflected wave is directed towards the *outside* of the crystal (Fig. 5.1.3.3*b*). The cosines defined by (5.1.3.2) are now positive for γ_o and negative for γ_h. The asymmetry factor is therefore also negative.

5.1.3.3. *Middle of the reflection domain*

It will be apparent from the equations given later that the incident wavevector corresponding to the middle of the reflection domain is, in both cases, **OI**, where *I* is the intersection of the normal to the crystal surface drawn from the Lorentz point, L_o, with T_o' (Figs. 5.1.3.4 and 5.1.3.5), while, according to Bragg's law, it should be $\mathbf{OL}_a$. The angle $\Delta\theta$ between the incident wavevectors $\mathbf{OL}_a$ and **OI**, corresponding to the middle of the reflecting domain according to the geometrical and dynamical theories, respectively, is

$$\Delta\theta_o = \overline{L_a I}/k = R\lambda^2 F_o(1-\gamma)/(2\pi V \sin 2\theta). \tag{5.1.3.4}$$

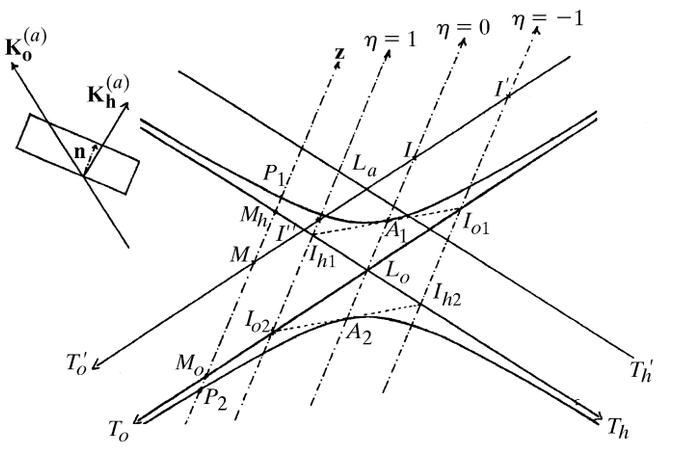

Fig. 5.1.3.4. Boundary conditions at the entrance surface for transmission geometry.

In the Bragg case, the asymmetry ratio γ is negative and $\Delta\theta_o$ is never equal to zero. This difference in Bragg angle between the two theories is due to the refraction effect, which is neglected in geometrical theory. In the Laue case, $\Delta\theta_o$ is equal to zero for symmetric reflections ($\gamma = 1$).

5.1.3.4. *Deviation parameter*

The solutions of dynamical theory are best described by introducing a reduced parameter called the *deviation parameter*,

$$\eta = (\Delta\theta - \Delta\theta_o)/\delta, \tag{5.1.3.5}$$

where

$$\delta = R\lambda^2|C|(|\gamma|F_h F_{\bar{h}})^{1/2}/(\pi V \sin 2\theta), \tag{5.1.3.6}$$

whose real part is equal to the half width of the rocking curve (Sections 5.1.6 and 5.1.7). The width 2δ of the rocking curve is sometimes called the *Darwin width*.

The definition (5.1.3.5) of the deviation parameter is independent of the geometrical situation (reflection or transmission case); this is not followed by some authors. The present convention has the advantage of being quite general.

In an absorbing crystal, $\eta, \Delta\theta_o$ and δ are complex, and it is the real part, $\Delta\theta_{or}$, of $\Delta\theta_o$ which has the geometrical interpretation given in Section 5.1.3.3. One obtains

$$\begin{aligned} &\eta = \eta_r + i\eta_i \\ &\eta_r = (\Delta\theta - \Delta\theta_{or})/\delta_r;\ \eta_i = A\eta_r + B \\ &A = -\tan\beta \\ &B = \left\{\chi_{io}/\left[|C|(|\chi_h\chi_{\bar{h}}|)^{1/2}\cos\beta\right]\right\}(1-\gamma)/2(|\gamma|)^{1/2}, \end{aligned} \tag{5.1.3.7}$$

where β is the phase angle of $(\chi_h\chi_{\bar{h}})^{1/2}$ [or that of $(F_h F_{\bar{h}})^{1/2}$].

5.1.3.5. *Pendellösung and extinction distances*

Let

$$\Lambda_o = \pi V(\gamma_o|\gamma_h|)^{1/2}/[R\lambda|C|(F_h F_{\bar{h}})^{1/2}]. \tag{5.1.3.8}$$

This length plays a very important role in the dynamical theory of diffraction by both perfect and deformed crystals. For example, it is 15.3 μm for the 220 reflection of silicon, with Mo $K\alpha$ radiation and a symmetric reflection.

In *transmission* geometry, it gives the period of the interference between the two excited wavefields which constitutes the *Pendellösung* effect first described by Ewald (1917) (see Section

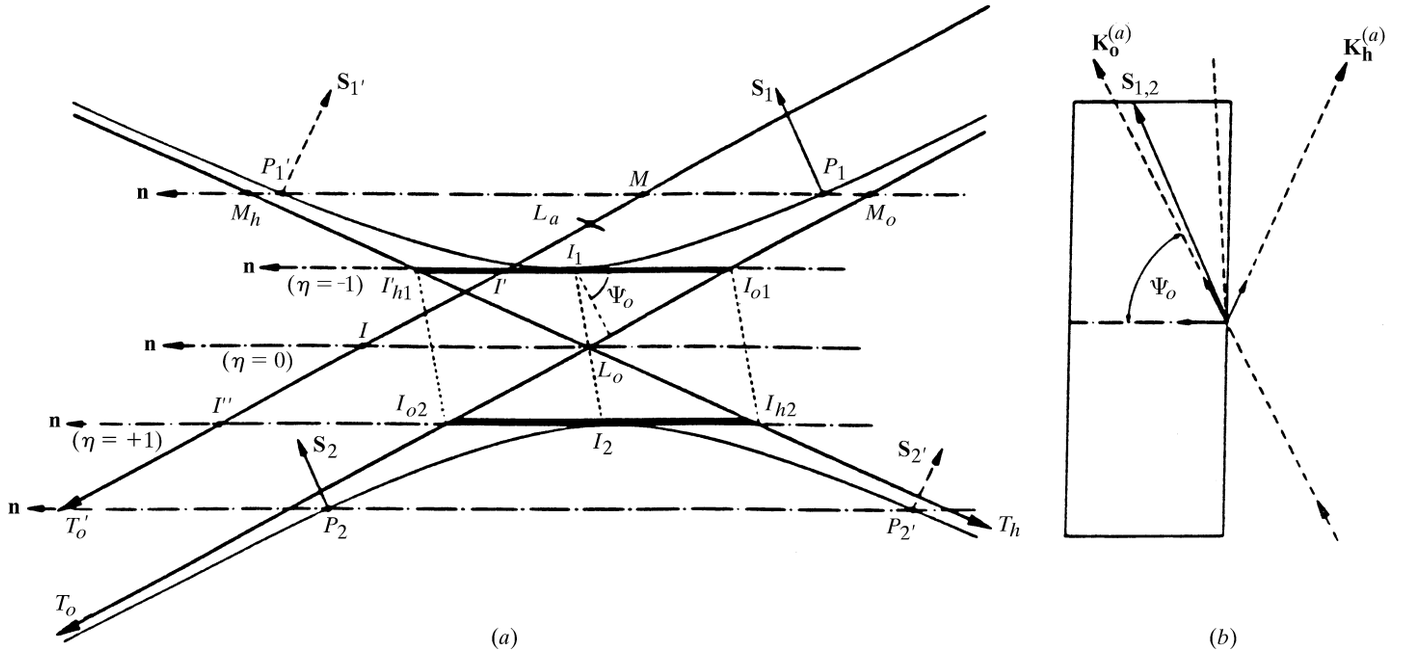

Fig. 5.1.3.5. Boundary conditions at the entrance surface for reflection geometry. (*a*) Reciprocal space; (*b*) direct space.

5.1.6.3); Λ_o in this case is called the *Pendellösung distance*, denoted Λ_L hereafter. Its geometrical interpretation, in the zero-absorption case, is the inverse of the diameter A_2A_1 of the dispersion surface in a direction defined by the cosines γ_h and γ_o with respect to the reflected and incident directions, respectively (Fig. 5.1.3.4). It reduces to the inverse of $A_{o2}A_{o1}$ (5.1.2.23) in the symmetric case.

In *reflection* geometry, it gives the absorption distance in the total-reflection domain and is called the *extinction* distance, denoted Λ_B (see Section 5.1.7.1). Its geometrical interpretation in the zero-absorption case is the inverse of the length $I_{o1}I_{h1} = I_{h2}I_{o2}$, Fig. 5.1.3.5.

In a *deformed* crystal, if distortions are of the order of the width of the rocking curve over a distance Λ_o, the crystal is considered to be slightly deformed, and ray theory (Penning & Polder, 1961; Kato, 1963, 1964*a*,*b*) can be used to describe the propagation of wavefields. If the distortions are larger, new wavefields may be generated by interbranch scattering (Authier & Balibar, 1970) and generalized dynamical diffraction theory such as that developed by Takagi (1962, 1969) should be used.

Using (5.1.3.8), expressions (5.1.3.5) and (5.1.3.6) can be rewritten in the very useful form:

$$\begin{aligned}\eta &= (\Delta\theta - \Delta\theta_o)\Lambda_o \sin 2\theta/(\lambda|\gamma_h|),\\ \delta &= \lambda|\gamma_h|/(\Lambda_o \sin 2\theta).\end{aligned} \tag{5.1.3.9}$$

The order of magnitude of the Darwin width 2δ ranges from a fraction of a second of an arc to ten or more seconds, and increases with increasing wavelength and increasing structure factor. For example, for the 220 reflection of silicon and Cu $K\alpha$ radiation, it is 5.2 seconds.

5.1.3.6. *Solution of the dynamical theory*

The coordinates of the tie points excited by the incident wave are obtained by looking for the intersection of the dispersion surface, (5.1.2.22), with the normal **Mz** to the crystal surface (Figs. 5.1.3.4 and 5.1.3.5). The ratio ξ of the amplitudes of the waves of the corresponding wavefields is related to these coordinates by (5.1.2.24) and is found to be

$$\begin{aligned}\xi_j &= D_{hj}/D_{oj}\\ &= -\mathrm{S}(C)\mathrm{S}(\gamma_h)[(F_hF_{\bar{h}})^{1/2}/F_{\bar{h}}]\\ &\quad\times\left\{\eta \pm \left[\eta^2 + \mathrm{S}(\gamma_h)\right]^{1/2}\right\}/(|\gamma|)^{1/2},\end{aligned} \tag{5.1.3.10}$$

where the plus sign corresponds to a tie point on branch 1 ($j = 1$) and the minus sign to a tie point on branch 2 ($j = 2$), and $\mathrm{S}(\gamma_h)$ is the sign of γ_h (+1 in transmission geometry, -1 in reflection geometry).

5.1.3.7. *Geometrical interpretation of the solution in the zero-absorption case*

5.1.3.7.1. *Transmission geometry*

In this case (Fig. 5.1.3.4) $\mathrm{S}(\gamma_h)$ is +1 and (5.1.3.10) may be written

$$\xi_j = -\mathrm{S}(C)\left[\eta \pm (\eta^2 + 1)^{1/2}\right]/\gamma^{1/2}. \tag{5.1.3.11}$$

Let A_1 and A_2 be the intersections of the normal to the crystal surface drawn from the Lorentz point L_o with the two branches of the dispersion surface (Fig. 5.1.3.4). From Sections 5.1.3.3 and 5.1.3.4, they are the tie points excited for $\eta = 0$ and correspond to the middle of the reflection domain. Let us further consider the tangents to the dispersion surface at A_1 and A_2 and let I_{o1}, I_{o2} and I_{h1}, I_{h2} be their intersections with T_o and T_h, respectively. It can be shown that $\overline{I_{o1}I_{h2}}$ and $\overline{I_{o2}I_{h1}}$ intersect the dispersion surface at the tie points excited for $\eta = -1$ and $\eta = +1$, respectively, and that the *Pendellösung* distance $\Lambda_L = 1/\overline{A_2A_1}$, the width of the rocking curve $2\delta = \overline{I_{o1}I_{o2}}/k$ and the deviation parameter $\eta = \overline{M_oM_h}/\overline{A_2A_1}$, where M_o and M_h are the intersections of the normal to the crystal surface drawn from the extremity of any incident wavevector **OM** with T_o and T_h, respectively.

5.1.3.7.2. *Reflection geometry*

In this case (Fig. 5.1.3.5) $S(\gamma_h)$ is now -1 and (5.1.3.10) may be written

$$\xi_j = S(C)\left[\eta \pm (\eta^2 - 1)^{1/2}\right]/|\gamma|^{1/2}. \quad (5.1.3.12)$$

Now, let I_1 and I_2 be the points of the dispersion surface where the tangent is parallel to the normal to the crystal surface, and further let I_{o1}, I_{h1}, I' and I_{o2}, I_{h2}, I'' be the intersections of these two tangents with T_o, T_h and T'_o, respectively. For an incident wave of wavevector **OM** where M lies between I' and I'', the normal to the crystal surface drawn from M has no real intersection with the dispersion surface and $\overline{I'I''}$ defines the total-reflection domain. The tie points I_1 and I_2 correspond to $\eta = -1$ and $\eta = +1$, respectively, the extinction distance $\Lambda_L = 1/\overline{I_{o1}I_{h1}}$, the width of the total-reflection domain $2\delta = \overline{I_{o1}I_{o2}}/k = \overline{I'I''}/k$ and the deviation parameter $\eta = -\overline{M_oM_h}/\overline{I_{o1}I_{h1}}$, where M_o and M_h are the intersections with T_o and T_h of the normal to the crystal surface drawn from the extremity of any incident wavevector **OM**.

5.1.4. Standing waves

The various waves in a wavefield are coherent and interfere. In the two-beam case, the intensity of the wavefield, using (5.1.2.14) and (5.1.2.24), is

$$|D|^2 = |D_o|^2 \exp(4\pi \mathbf{K}_{oi} \cdot \mathbf{r}) \times [1 + |\xi|^2 + 2C|\xi| \cos 2\pi(\mathbf{h} \cdot \mathbf{r} + \Psi)], \quad (5.1.4.1)$$

where Ψ is the phase of ξ,

$$\xi = |\xi| \exp(i\Psi). \quad (5.1.4.2)$$

Equation (5.1.4.1) shows that the interference between the two waves is the origin of *standing waves*. The corresponding nodes lie on planes such that $\mathbf{h} \cdot \mathbf{r}$ is a constant. These planes are therefore parallel to the diffraction planes and their periodicity is equal to d_{hkl} (defined in the caption for Fig. 5.1.2.1*a*). Their position within the unit cell is given by the value of the phase Ψ.

In the Laue case, Ψ is equal to $\pi + \varphi_h$ for branch 1 and to φ_h for branch 2, where φ_h is the phase of the structure factor, (5.1.2.6). This means that the *nodes* of standing waves lie on the maxima of the *hkl* Fourier component of the electron density for branch 1 while the *anti-nodes* lie on the maxima for branch 2.

In the Bragg case, Ψ varies continuously from $\pi + \varphi_h$ to φ_h as the angle of incidence is varied from the low-angle side to the high-angle side of the reflection domain by rocking the crystal. The nodes lie on the maxima of the *hkl* Fourier components of the electron density on the low-angle side of the rocking curve. As the crystal is rocked, they are progressively shifted by half a lattice spacing until the anti-nodes lie on the maxima of the electron density on the high-angle side of the rocking curve.

Standing waves are the origin of the phenomenon of anomalous absorption, which is one of the specific properties of wavefields (Section 5.1.5). Anomalous scattering is also used for the location of atoms in the unit cell at the vicinity of the crystal surface: when X-rays are absorbed, fluorescent radiation and photoelectrons are emitted. Detection of this emission for a known angular position of the crystal with respect to the rocking curve and therefore for a known value of the phase Ψ enables the emitting atom within the unit cell to be located. The principle of this method is due to Batterman (1964, 1969). For reviews, see Golovchenko *et al.* (1982), Materlik & Zegenhagen (1984), Kovalchuk & Kohn (1986), Bedzyk (1988), Authier (1989), and Zegenhagen (1993).

5.1.5. Anomalous absorption

It was shown in Section 5.1.2.2 that the wavevectors of a given wavefield all have the same imaginary part (5.1.2.17) and therefore the same absorption coefficient μ (5.1.2.19). Borrmann (1950, 1954) showed that this coefficient is much smaller than the normal one (μ_o) for wavefields whose tie points lie on branch 1 of the dispersion surface and much larger for wavefields whose tie points lie on branch 2. The former case corresponds to the *anomalous transmission effect*, or *Borrmann effect*. As in favourable cases the minimum absorption coefficient may be as low as a few per cent of μ_o, this effect is very important from both a fundamental and a practical point of view.

The physical interpretation of the Borrmann effect is to be found in the standing waves described in Section 5.1.4. When the nodes of the electric field lie on the planes corresponding to the maxima of the *hkl* component of the electron density, the wavefields are absorbed anomalously less than when there is no diffraction. Just the opposite occurs for branch 2 wavefields, whose anti-nodes lie on the maxima of the electron density and which are absorbed more than normal.

The effective absorption coefficient μ is related to the imaginary part of the wavevectors through (5.1.2.19),

$$\mu = -4\pi\gamma_o K_{oi},$$

and to the imaginary part of the ratio of the amplitude of the reflected to the incident wave through

$$\mu = \mu_o - 4\pi X_{oi}, \quad (5.1.5.1)$$

where X_{oi} is the imaginary part of X_o, which, using (5.1.2.24) and (5.1.3.10), is given by

$$X_o = R\lambda|C|S(\gamma_h)(F_hF_{\bar{h}})^{1/2} \times \{\eta \pm [\eta^2 + S(\gamma_h)]^{1/2}\}/\left[2\pi V(|\gamma|)^{1/2}\right]. \quad (5.1.5.2)$$

Taking the upper sign (+) for the $\pm$ term corresponds to tie points on branch 1 and taking the lower sign $(-)$ corresponds to tie points on branch 2.

The calculation of the imaginary part X_{oi} is different in the Laue and in the Bragg cases. In the former case, the imaginary part of $(\eta^2 + 1)^{1/2}$ is small and can be approximated while in the latter, the imaginary part of $(\eta^2 - 1)^{1/2}$ is large when the real part of the deviation parameter, η_r, lies between 1 and -1, and cannot be calculated using the same approximation.

5.1.6. Intensities of plane waves in transmission geometry

5.1.6.1. *Absorption coefficient*

In transmission geometry, the imaginary part of X_o is small and, using a first-order approximation for the expansion of $(\eta^2 + 1)^{1/2}$, (5.1.5.1) and (5.1.5.2), the effective absorption coefficient in the absorption case is

$$\mu_j = \mu_o\left[\tfrac{1}{2}(1 + \gamma^{-1}). \mp \frac{(\eta_r/2)(1 - \gamma^{-1}) + |C|(\gamma^{-1})^{1/2}|F_{ih}/F_{io}| \cos\varphi}{(\eta_r^2 + 1)^{1/2}}\right], \quad (5.1.6.1)$$

where $\varphi = \varphi_{rh} - \varphi_{ih}$ is the phase difference between F_{rh} and F_{ih} [equation (5.1.2.10)], the upper sign $(-)$ for the $\mp$ term corresponds to branch 1 and the lower sign (+) corresponds to branch 2 of the dispersion surface. In the symmetric Laue case ($\gamma = 1$, reflecting planes normal to the crystal surface), equation (5.1.6.1) reduces to

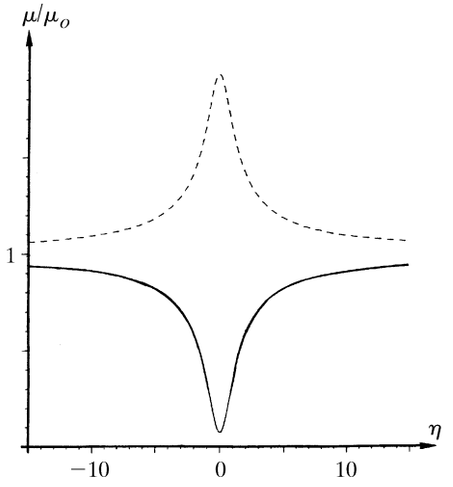

Fig. 5.1.6.1. Variation of the effective absorption with the deviation parameter in the transmission case for the 400 reflection of GaAs using Cu $K\alpha$ radiation. Solid curve: branch 1; broken curve: branch 2.

$$\mu_j = \mu_o \left[1 \mp \frac{|C||F_{ih}/F_{io}| \cos\varphi}{(\eta_r^2 + 1)^{1/2}} \right].$$

Fig. 5.1.6.1 shows the variations of the effective absorption coefficient μ_j with η_r for wavefields belonging to branches 1 and 2 in the case of the 400 reflection of GaAs with Cu $K\alpha$ radiation. It can be seen that for $\eta_r = 0$ the absorption coefficient for branch 1 becomes significantly smaller than the normal absorption coefficient, μ_o. The minimum absorption coefficient, $\mu_o(1 - |CF_{ih}/F_{io}| \cos\varphi)$, depends on the nature of the reflection through the structure factor and on the temperature through the Debye–Waller factor included in F_{ih} [equation (5.1.2.10*b*)] (Ohtsuki, 1964, 1965). For instance, in diamond-type structures, it is smaller for reflections with even indices than for reflections with odd indices. The influence of temperature is very important when $|F_{ih}/F_{io}|$ is close to one; for example, for germanium 220 and Mo $K\alpha$ radiation, the minimum absorption coefficient at 5 K is reduced to about 1% of its normal value, μ_o (Ludewig, 1969).

5.1.6.2. *Boundary conditions for the amplitudes at the entrance surface – intensities of the reflected and refracted waves*

Let us consider an infinite plane wave incident on a crystal plane surface of infinite lateral extension. As has been shown in Section 5.1.3, two wavefields are excited in the crystal, with tie points P_1 and P_2, and amplitudes D_{o1}, D_{h1} and D_{o2}, D_{h2}, respectively. Maxwell's boundary conditions (see Section A5.1.1.2 of the Appendix) imply continuity of the tangential component of the electric field and of the normal component of the electric displacement across the boundary. Because the index of refraction is so close to unity, one can assume to a very good approximation that there is continuity of the three components of both the electric field and the electric displacement. As a consequence, it can easily be shown that, *along the entrance surface*, for all components of the electric displacement

$$\begin{aligned} D_o^{(a)} &= D_{o1} + D_{o2} \\ 0 &= D_{h1} + D_{h2}, \end{aligned} \qquad (5.1.6.2)$$

where $D_o^{(a)}$ is the amplitude of the incident wave.

Using (5.1.3.11), (5.1.5.2) and (5.1.6.2), it can be shown that the *intensities* of the four waves are

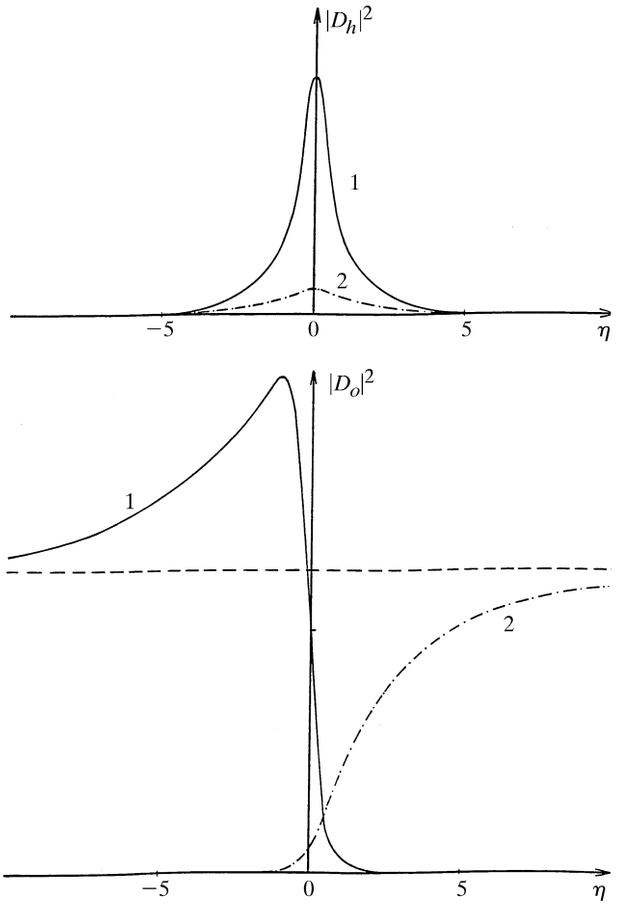

Fig. 5.1.6.2. Variation of the intensities of the reflected and refracted waves in an absorbing crystal for the 220 reflection of Si using Mo $K\alpha$ radiation, $t = 1$ mm ($\mu t = 1.42$). Solid curve: branch 1; dashed curve: branch 2.

$$\begin{aligned} |D_{oj}|^2 &= |D_o^{(a)}|^2 \exp(-\mu_j z/\gamma_o) \left[(1 + \eta_r^2)^{1/2} \mp \eta_r \right]^2 \\ &\quad \times [4(1 + \eta_r^2)]^{-1}, \\ |D_{hj}|^2 &= |D_o^{(a)}|^2 \exp(-\mu_j z/\gamma_o) |F_h/F_{\bar{h}}| [4\gamma(1 + \eta_r^2)]^{-1}; \end{aligned} \qquad (5.1.6.3)$$

top sign: $j = 1$; bottom sign: $j = 2$.

Fig. 5.1.6.2 represents the variations of these four intensities with the deviation parameter. Far from the reflection domain, $|D_{h1}|^2$ and $|D_{h2}|^2$ tend toward zero, as is normal, while

$$|D_{o1}|^2 \gg |D_{o2}|^2 \text{ for } \eta_r \Rightarrow -\infty,$$
$$|D_{o1}|^2 \ll |D_{o2}|^2 \text{ for } \eta_r \Rightarrow +\infty.$$

This result shows that the wavefield of highest intensity 'jumps' from one branch of the dispersion surface to the other across the reflection domain. This is an important property of dynamical theory which also holds in the Bragg case and when a wavefield crosses a highly distorted region in a deformed crystal [the so-called *interbranch scattering*: see, for instance, Authier & Balibar (1970) and Authier & Malgrange (1998)].

5.1.6.3. *Boundary conditions at the exit surface*

5.1.6.3.1. *Wavevectors*

When a wavefield reaches the exit surface, it breaks up into its two constituent waves. Their wavevectors are obtained by applying

again the condition of the continuity of their tangential components along the crystal surface. The extremities, M_j and N_j, of these wavevectors

$$\mathbf{OM}_j = \mathbf{K}_{\mathbf{o}j}^{(d)} \qquad \mathbf{HN}_j = \mathbf{K}_{\mathbf{h}j}^{(d)}$$

lie at the intersections of the spheres of radius k centred at O and H, respectively, with the normal $\mathbf{n}'$ to the crystal exit surface drawn from P_j ($j = 1$ and 2) (Fig. 5.1.6.3).

If the crystal is wedge-shaped and the normals $\mathbf{n}$ and $\mathbf{n}'$ to the entrance and exit surfaces are not parallel, the wavevectors of the waves generated by the two wavefields are not parallel. This effect is due to the refraction properties associated with the dispersion surface.

5.1.6.3.2. *Amplitudes – Pendellösung*

We shall assume from now on that the crystal is plane parallel. Two wavefields arrive at any point of the exit surface. Their constituent waves interfere and generate emerging waves in the refracted and reflected directions (Fig. 5.1.6.4). Their respective

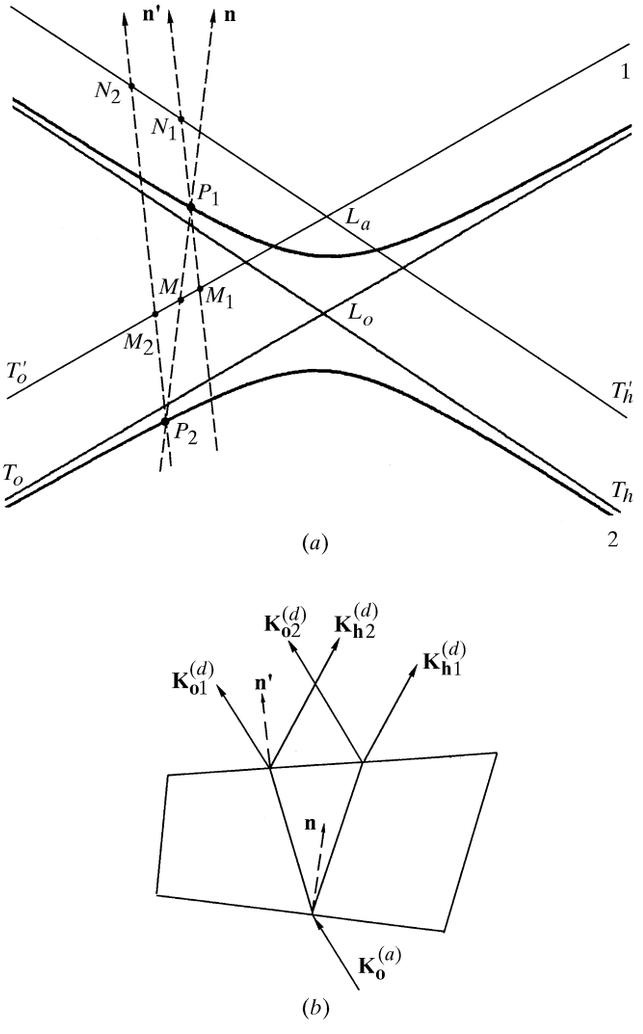

Fig. 5.1.6.3. Boundary condition for the wavevectors at the exit surface. (*a*) Reciprocal space. The wavevectors of the emerging waves are determined by the intersections M_1, M_2, N_1 and N_2 of the normals $\mathbf{n}'$ to the exit surface, drawn from the tie points P_1 and P_2 of the wavefields, with the tangents T'_o and T'_h to the spheres centred at O and H and of radius k, respectively. (*b*) Direct space.

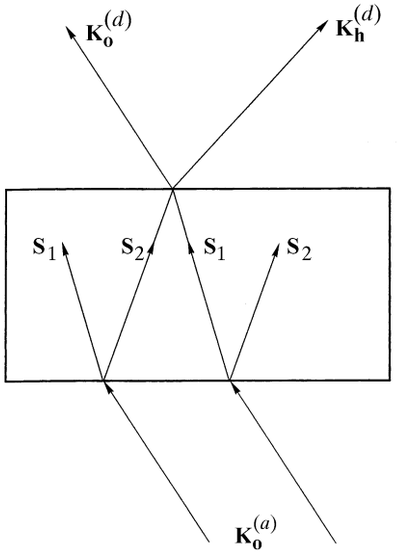

Fig. 5.1.6.4. Decomposition of a wavefield into its two components when it reaches the exit surface. $\mathbf{S}_1$ and $\mathbf{S}_2$ are the Poynting vectors of the two wavefields propagating in the crystal belonging to branches 1 and 2 of the dispersion surface, respectively, and interfering at the exit surface.

amplitudes are given by the boundary conditions

$$\begin{aligned} D_o^{(d)} \exp(-2\pi i \mathbf{K}_{\mathbf{o}}^{(d)} \cdot \mathbf{r}) &= D_{o1} \exp(-2\pi i \mathbf{K}_{\mathbf{o}1} \cdot \mathbf{r}) \\ &\quad + D_{o2} \exp(-2\pi i \mathbf{K}_{\mathbf{o}2} \cdot \mathbf{r}) \\ D_h^{(d)} \exp(-2\pi i \mathbf{K}_{\mathbf{h}}^{(d)} \cdot \mathbf{r}) &= D_{h1} \exp(-2\pi i \mathbf{K}_{\mathbf{h}1} \cdot \mathbf{r}) \\ &\quad + D_{h2} \exp(-2\pi i \mathbf{K}_{\mathbf{h}2} \cdot \mathbf{r}), \end{aligned} \tag{5.1.6.4}$$

where $\mathbf{r}$ is the position vector of a point on the exit surface, the origin of phases being taken at the entrance surface.

In a plane-parallel crystal, (5.1.6.4) reduces to

$$\begin{aligned} D_o^{(d)} &= D_{o1} \exp\big(-2\pi i \overline{MP_1} \cdot t\big) + D_{o2} \exp\big(-2\pi i \overline{MP_2} \cdot t\big) \\ D_h^{(d)} &= D_{h1} \exp\big(-2\pi i \overline{MP_1} \cdot t\big) + D_{h2} \exp\big(-2\pi i \overline{MP_2} \cdot t\big), \end{aligned}$$

where t is the crystal thickness.

In a *non-absorbing* crystal, the amplitudes squared are of the form

$$\big|D_o^{(d)}\big|^2 = |D_{o1}|^2 + |D_{o2}|^2 + 2D_{o1}D_{o2} \cos 2\pi \overline{P_2P_1} t.$$

This expression shows that the intensities of the refracted and reflected beams are oscillating functions of crystal thickness. The period of the oscillations is called the *Pendellösung* distance and is

$$\Lambda = 1/\overline{P_2P_1} = \Lambda_L/(1 + \eta_r^2)^{1/2}.$$

5.1.6.4. *Reflecting power*

For an *absorbing* crystal, the intensities of the reflected and refracted waves are

$$\begin{aligned} \big|D_o^{(d)}\big|^2 &= \big|D_o^{(a)}\big|^2 A_\eta \Big\{ \cosh(2v + \mu_a t). \\ &\qquad + \cos\Big[2\pi t \Lambda^{-1} - 2\eta_i (1 + \eta_r^2)^{-1/2}\Big] \Big\} \\ \Big|D_h^{(d)}\Big|^2 &= \big|D_o^{(a)}\big|^2 |F_h/F_{\bar{h}}| \gamma^{-1} A_\eta \big[\cosh(\mu_a t) - \cos(2\pi t \Lambda^{-1})\big], \end{aligned} \tag{5.1.6.5}$$

where

$$A_\eta = \left[\exp -\mu_o t(\gamma_o^{-1} + \gamma_h^{-1})\right]/2(1+\eta_r^2),$$
$$\mu_a = \mu_j\Big[1/2(\gamma_o^{-1} - \gamma_h^{-1})\eta_r + |C||F_{ih}/F_{io}|\cos\varphi/(\gamma_o\gamma_h)^{1/2}\Big](1+\eta_r^2)^{-1/2},$$
$$v = \operatorname{arg\,sinh}\eta_r$$

and μ_j is given by equation (5.1.6.1).

Depending on the absorption coefficient, the cosine terms are more or less important relative to the hyperbolic cosine term and the oscillations due to *Pendellösung* have more or less contrast.

For a non-absorbing crystal, these expressions reduce to

$$\left|D_o^{(d)}\right|^2 = \left|D_o^{(a)}\right|^2\left[\frac{1+2\eta^2+\cos(2\pi t\Lambda^{-1})}{2(1+\eta_r^2)}\right],$$
$$\left|D_h^{(d)}\right|^2 = \left|D_o^{(a)}\right|^2\left[\frac{1-\cos(2\pi t\Lambda^{-1})}{2\gamma(1+\eta_r^2)}\right]. \qquad (5.1.6.6)$$

What is actually measured in a counter receiving the reflected or the refracted beam is the *reflecting power*, namely the ratio of the energy of the reflected or refracted beam on the one hand and the energy of the incident beam on the other. The energy of a beam is obtained by multiplying its intensity by its cross section. If l is the width of the trace of the beam on the crystal surface, the cross sections of the incident (or refracted) and reflected beams are proportional to (Fig. 5.1.6.5) $l_o = l\gamma_o$ and $l_h = l\gamma_h$, respectively.

The reflecting powers are therefore:

$$\text{Refracted beam: } I_o = l_o\left|D_o^{(d)}\right|^2\Big/ l_o\left|D_o^{(a)}\right|^2 = \left|D_o^{(d)}\right|^2\Big/\left|D_o^{(a)}\right|^2,$$
$$\text{Reflected beam: } I_h = l_h\left|D_h^{(d)}\right|^2\Big/ l_o\left|D_o^{(a)}\right|^2 = \gamma\left|D_h^{(d)}\right|^2\Big/\left|D_o^{(a)}\right|^2. \qquad (5.1.6.7)$$

Using (5.1.6.6), it is easy to check that $I_o + I_h = 1$ in the non-absorbing case; that is, that conservation of energy is satisfied. Equations (5.1.6.6) show that there is a periodic exchange of energy between the refracted and the reflected waves as the beam penetrates the crystal; this is why Ewald introduced the expression *Pendellösung*.

The oscillations in the rocking curve were first observed by Lefeld-Sosnowska & Malgrange (1968, 1969). Their periodicity can be used for accurate measurements of the form factor [see, for instance, Bonse & Teworte (1980)]. Fig. 5.1.6.6 shows the shape of the rocking curve for various values of t/Λ_L.

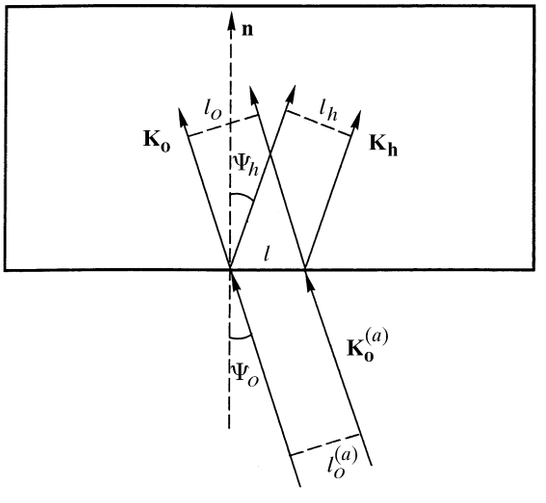

Fig. 5.1.6.5. Cross sections of the incident, $\mathbf{K}_\mathbf{o}^{(a)}$, refracted, $\mathbf{K_o}$, and reflected, $\mathbf{K_h}$, waves.

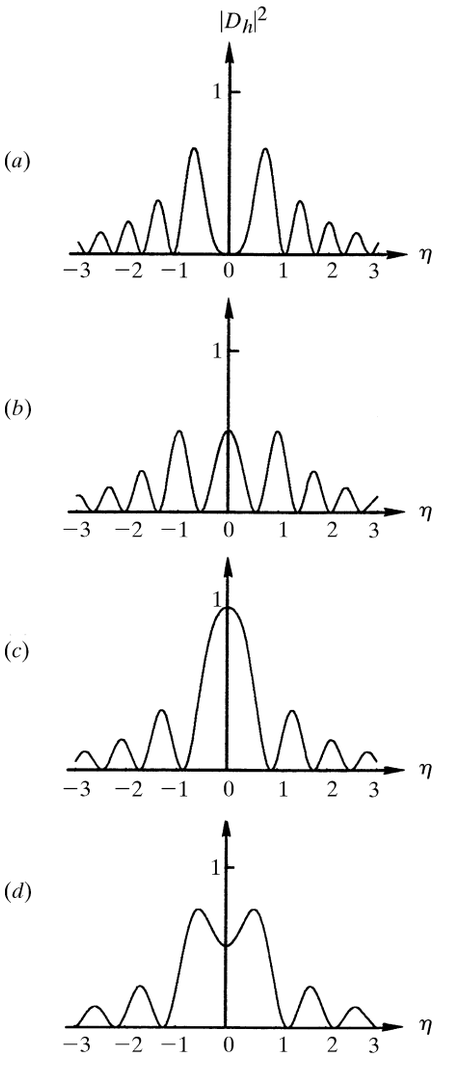

Fig. 5.1.6.6. Theoretical rocking curves in the transmission case for non-absorbing crystals and for various values of t/Λ_L: (*a*) $t/\Lambda_L = 1.25$; (*b*) $t/\Lambda_L = 1.5$; (*c*) $t/\Lambda_L = 1.75$; (*d*) $t/\Lambda_L = 2.0$.

The *width at half-height of the rocking curve*, averaged over the *Pendellösung* oscillations, corresponds in the non-absorbing case to $\Delta\eta = 2$, that is, to $\Delta\theta = 2\delta$, where δ is given by (5.1.3.6).

5.1.6.5. *Integrated intensity*

5.1.6.5.1. *Non-absorbing crystals*

The integrated intensity is the ratio of the total energy recorded in the counter when the crystal is rocked to the intensity of the incident beam. It is proportional to the area under the line profile:

$$I_{hi} = \int_{-\infty}^{+\infty} I_h\, \mathrm{d}(\Delta\theta). \qquad (5.1.6.8)$$

The integration was performed by von Laue (1960). Using (5.1.3.5), (5.1.6.6) and (5.1.6.7) gives

$$I_{hi} = A\int_0^{2\pi t\Lambda_L^{-1}} J_0(z)\, \mathrm{d}z,$$

where $J_0(z)$ is the zeroth-order Bessel function and

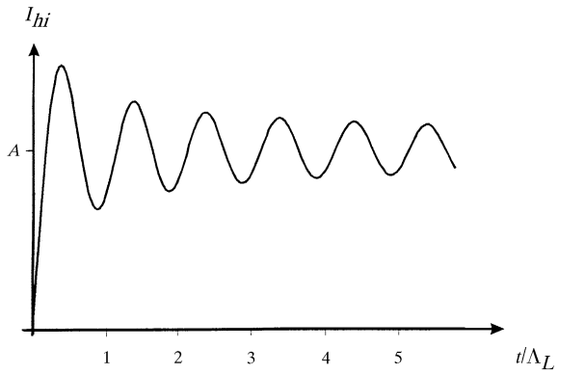

Fig. 5.1.6.7. Variations with crystal thickness of the integrated intensity in the transmission case (no absorption) (arbitrary units). The expression for A is given in the text.

$$A = \frac{R\lambda^2 |CF_h| (\gamma)^{1/2}}{2V \sin 2\theta}.$$

Fig. 5.1.6.7 shows the variations of the integrated intensity with t/Λ_L.

5.1.6.5.2. *Absorbing crystals*

The integration was performed for absorbing crystals by Kato (1955). The integrated intensity in this case is given by

$$I_{hi} = A|F_h/F_{\bar{h}}| \exp\left[-1/2\mu_o t(\gamma_o^{-1} + \gamma_h^{-1})\right] \times \left[\int_0^{2\pi t\Lambda_L^{-1}} J_0(z)\, \mathrm{d}z - 1 + I_0(\zeta)\right],$$

where

$$\zeta = \mu_o t \left\{ \left[|C|^2 |F_{ih}/F_{io}|^2 \cos^2 \varphi + (\gamma_h - \gamma_o)/(4\gamma_o\gamma_h) \right] / (\gamma_o\gamma_h) \right\}^{1/2}$$

and $I_0(\zeta)$ is a modified Bessel function of zeroth order.

5.1.6.6. *Thin crystals – comparison with geometrical theory*

Using (5.1.6.6) and (5.1.6.7), the reflecting power of the reflected beam may also be written

$$I_h = \pi^2 t^2 \Lambda_o^{-2} f(\eta),$$

where

$$f(\eta) = \left[\frac{\sin U(1+\eta^2)^{1/2}}{U(1+\eta^2)^{1/2}} \right]^2$$

and

$$U = \pi t \Lambda_o^{-1}.$$

When $t\Lambda_o^{-1}$ is very small, $f(\eta)$ tends asymptotically towards the function

$$f_1(\eta) = \left[\frac{\sin U\eta}{U\eta} \right]^2$$

and I_h towards the value given by geometrical theory. The condition for geometrical theory to apply is, therefore, that the crystal thickness be much smaller than the *Pendellösung* distance. In practice, the two theories agree to within a few per cent for a crystal thickness smaller than or equal to a third of the *Pendellösung* distance [see Authier & Malgrange (1998)].

5.1.7. Intensity of plane waves in reflection geometry

5.1.7.1. *Thick crystals*

5.1.7.1.1. *Non-absorbing crystals*

Rocking curve. The geometrical construction in Fig. 5.1.3.5 shows that, in the Bragg case, the normal to the crystal surface drawn from the extremity of the incident wavevector intersects the dispersion surface either at two points of the same branch, P_1, P_1', for branch 1, P_2, P_2' for branch 2, or at imaginary points. It was shown in Section 5.1.2.6 that the propagation of the wavefields inside the crystal is along the normal to the dispersion surface at the corresponding tie points. Fig. 5.1.3.5 shows that this direction is oriented towards the outside of the crystal for tie points P_1' and P_2'. In a very thick crystal, these wavefields cannot exist because there is always a small amount of absorption. One concludes that in the thick-crystal case and in reflection geometry, only one wavefield is excited inside the crystal. It corresponds to branch 1 on the low-angle side of the rocking curve and to branch 2 on the high-angle side. Using the same approximations as in Section 5.1.6.2, the amplitude $\mathbf{D}_\mathbf{h}^{(a)}$ of the wave reflected at the crystal surface is obtained by applying the boundary conditions, which are particularly simple in this case:

$$\mathbf{D_o} = \mathbf{D_o}^{(a)},\ \mathbf{D_h}^{(a)} = \mathbf{D_h}.$$

The reflecting power is given by an expression similar to (5.1.6.7):

$$I_h = |\gamma||\xi_j|^2,$$

where the expression for ξ_j is given by (5.1.3.12), and $j = 1$ or 2 depending on which wavefield propagates towards the inside of the crystal. When the normal to the entrance surface intersects the dispersion surface at imaginary points, *i.e.* when $-1 < \eta < +1$,

$$|\xi|^2 = |\gamma|^{-1},\ I_h = 1, \qquad (5.1.7.1)$$

and there is *total reflection.* Outside the total-reflection domain, the reflecting power is given by

$$I_h = \left[|\eta| - (\eta^2 - 1)^{1/2} \right]^2. \qquad (5.1.7.2)$$

The rocking curve has the well known top-hat shape (Fig. 5.1.7.1). Far from the total-reflection domain, the curve can be

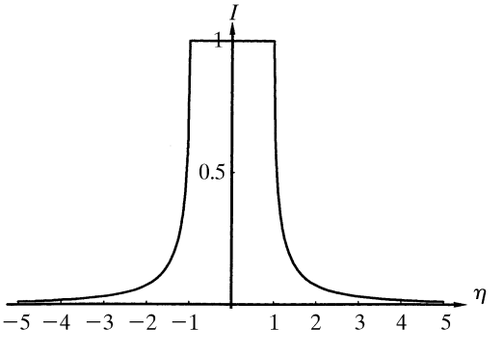

Fig. 5.1.7.1. Theoretical rocking curve in the reflection case for a non-absorbing thick crystal in terms of the deviation parameter.

approximated by the function

$$I_h \approx 1/(4\eta^2).$$

Width of the total-reflection domain. The width of the total-reflection domain is equal to $\Delta\eta = 2$ and its angular width is therefore equal, using (5.1.3.5), to 2δ, where δ is given by (5.1.3.6). It is proportional to the structure factor, the polarization factor C and the square root of the asymmetry factor $|\gamma|$. Using an asymmetric reflection, it is therefore possible to decrease the width at wish. This is used in monochromators to produce a pseudo plane wave [see, for instance, Kikuta & Kohra (1970)]. It is possible to deduce the value of the form factor from very accurate measurements of the rocking curve; see, for instance, Kikuta (1971).

Integrated intensity. The integrated intensity is defined by (5.1.6.8):

$$I_{hi} = 8\delta/3. \qquad (5.1.7.3)$$

Penetration depth. Within the domain of total reflection, there are two wavefields propagating inside the crystal with imaginary wavevectors, one towards the inside of the crystal and the other one in the opposite direction, so that they cancel out and, globally, no energy penetrates the crystal. The absorption coefficient of the waves penetrating the crystal is

$$\mu = -4\pi K_{oi}\gamma_o = 2\pi\gamma_o(1-\eta^2)^{1/2}/\Lambda_B, \qquad (5.1.7.4)$$

where Λ_B is the value taken by Λ_o [equation (5.1.3.8)] in the Bragg case.

The penetration depth is a minimum at the middle of the reflection domain and at this point it is equal to $\Lambda_B/2\pi$. This attenuation effect is called *extinction*, and Λ_B is called the *extinction length.* It is a specific property owing to the existence of wavefields. The resulting propagation direction of energy is parallel to the crystal surface, but with a cross section equal to zero: it is an *evanescent wave* [see, for instance, Cowan *et al.* (1986)].

5.1.7.1.2. *Absorbing crystals*

Rocking curve. Since the sign of γ is negative, $[\eta^2 + \mathrm{S}(\gamma h)]^{1/2}$ in (5.1.3.10) has a very large imaginary part when $|\eta_r| \leq 1$. It cannot be calculated using the same approximations as in the Laue case. Let us set

$$Z\exp(i\Psi') = \eta \mp (\eta^2 - 1)^{1/2}. \qquad (5.1.7.5)$$

The reflecting power is

$$I_h = (F_h/F_{\bar{h}})^{1/2}Z^2, \qquad (5.1.7.6)$$

where $Z = [L - (L^2-1)^{1/2}]^{1/2}, L = |\eta|^2 + \rho^2$ and $\rho = |\eta^2 - 1|$ is the modulus of expression (5.1.7.5) where the sign is chosen in such a way that Z is smaller than 1.

The expression for the reflected intensity in the absorbing Bragg case was first given by Prins (1930). The way of representing it given here was first used by Hirsch & Ramachandran (1950). The properties of the rocking curve have been described by Fingerland (1971).

There is no longer a total-reflection domain and energy penetrates the crystal at all incidence angles, although with a very high absorption coefficient within the domain $|\eta_r| \leq 1$. Fig. 5.1.7.2 gives an example of a rocking curve for a thick absorbing crystal. It was first observed by Renninger (1955). The shape is asymmetric and is due to the anomalous-absorption effect: it is lower than normal on the low-angle side, which is associated with wavefields belonging to branch 1 of the dispersion surface, and larger than normal on the high-angle side, which is associated with branch 2 wavefields. The amount of asymmetry depends on the value of the ratio A/B of the coefficients in the expression for the imaginary part

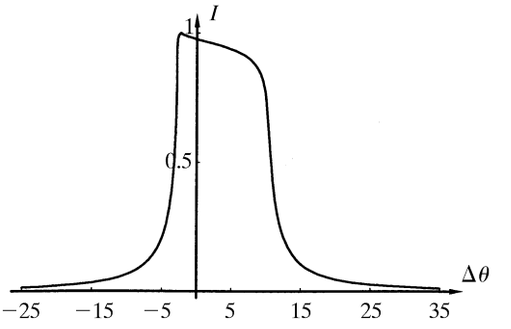

Fig. 5.1.7.2. Theoretical rocking curve in the reflection case for a thick absorbing crystal. The 400 reflection of GaAs using Cu $K\alpha$ radiation is shown.

of the deviation parameter in (5.1.3.7): the smaller this ratio, the more important the asymmetry.

Absorption coefficient. The effective absorption coefficient, taking into account both the Borrmann effect and extinction, is given by (Authier, 1986)

$$\mu = \mu_o + 2(|F_hF_{\bar{h}}|)^{1/2}\frac{R\lambda}{V(|\gamma|)^{1/2}}Z\sin(\beta+\Psi'),$$

where β is defined in equation (5.1.3.7) and Ψ' in equation (5.1.7.5), and where the sign is chosen in such a way that Z converges. Fig. 5.1.7.3 shows the variation of the penetration depth $z_o = \gamma_o/\mu$ with the deviation parameter.

5.1.7.2. *Thin crystals*

5.1.7.2.1. *Non-absorbing crystals*

Boundary conditions. If the crystal is thin, the wavefield created at the reflecting surface at A and penetrating inside can reach the back surface at B (Fig. 5.1.7.4*a*). The *incident* direction there points towards the *outside* of the crystal, while the *reflected* direction

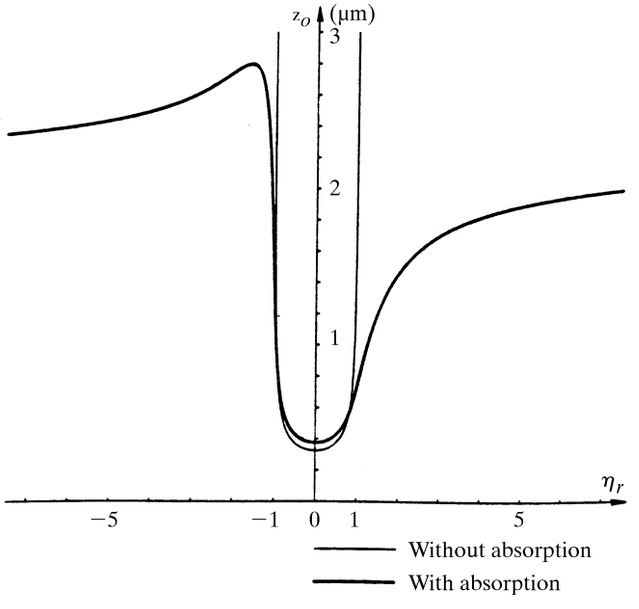

Fig. 5.1.7.3. Bragg case: thick crystals. Variation of the penetration depth with incidence angle (represented here by the dimensionless deviation parameter η). Thin curve: without absorption; thick curve: with absorption for the 400 reflection of GaAs using Cu $K\alpha$ radiation.

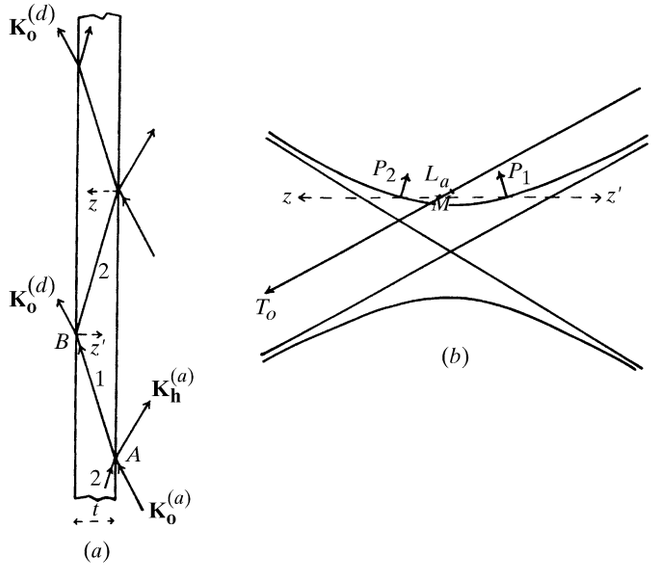

Fig. 5.1.7.4. Bragg case: thin crystals. Two wavefields propagate in the crystal. (*a*) Direct space; (*b*) reciprocal space.

points towards the inside. The wavefield propagating along *AB* will therefore generate at *B*:

(i) *a partially transmitted wave* outside the crystal, $\mathbf{D}_\mathbf{o}^{(d)} \exp(-2\pi i \mathbf{K}_\mathbf{o}^{(d)} \cdot \mathbf{r})$;

(ii) *a partially reflected wavefield* inside the crystal.

The corresponding tiepoints are obtained by applying the usual condition of the continuity of the tangential components of wavevectors (Fig. 5.1.7.4*b*). If the crystal is a plane-parallel slab, these points are *M* and P_2, respectively, and $\mathbf{K}_\mathbf{o}^{(d)} = \mathbf{K}_\mathbf{o}^{(a)}$.

The boundary conditions are then written:

(i) entrance surface:

$$D_{o1} + D_{o2} = D_o^{(a)}, \quad D_{h1} + D_{h2} = D_h^{(a)};$$

(ii) back surface:

$$D_{o1} \exp(-2\pi i \mathbf{K}_{\mathbf{o}1} \cdot \mathbf{r}) + D_{o2} \exp(-2\pi i \mathbf{K}_{\mathbf{o}2} \cdot \mathbf{r}) = D_o^{(a)} \exp\big(-2\pi i \mathbf{K}_\mathbf{o}^{(d)} \cdot \mathbf{r}\big),$$
$$D_{h1} \exp(-2\pi i \mathbf{K}_{\mathbf{h}1} \cdot \mathbf{r}) + D_{h2} \exp(-2\pi i \mathbf{K}_{\mathbf{h}2} \cdot \mathbf{r}) = 0.$$

Rocking curve. Using (5.1.3.10), it can be shown that the expressions for the intensities reflected at the entrance surface and transmitted at the back surface, I_h and I_o, respectively, are given by different expressions within total reflection and outside it:

(i) $|\eta| < 1$:

$$I_h = |\gamma| \frac{|D_h^{(a)}|^2}{|D_o^{(a)}|^2} = \frac{\cosh^2[\pi(t/\Lambda_B)(1-\eta^2)^{1/2}] - 1}{\cosh^2[\pi(t/\Lambda_B)(1-\eta^2)^{1/2}] - \eta^2}$$
$$I_o = \frac{|D_o^{(d)}|^2}{|D_o^{(a)}|^2} = \frac{1-\eta^2}{\cosh^2[\pi(t/\Lambda_B)(1-\eta^2)^{1/2}] - \eta^2}, \qquad (5.1.7.7a)$$

where Λ_B is the value taken by Λ_o [equation (5.1.3.8)] in the Bragg case.

There is no longer a total-reflection domain but the extinction effect still exists, as is shown by the hyperbolic cosine term. The maximum height of the rocking curve decreases as the thickness of the crystal decreases.

(ii) $|\eta| > 1$:

$$I_h = \frac{1 - \cos^2[\pi(t/\Lambda_B)(\eta^2-1)^{1/2}]}{\eta^2 - \cos^2[\pi(t/\Lambda_B)(\eta^2-1)^{1/2}]},$$
$$I_o = \frac{\eta^2 - 1}{\eta^2 - \cos^2[\pi(t/\Lambda_B)(\eta^2-1)^{1/2}]}. \qquad (5.1.7.7b)$$

The cosine terms show that the two wavefields propagating within the crystal interfere, giving rise to *Pendellösung* fringes in the rocking curve. These fringes were observed for the first time by Batterman & Hildebrandt (1967, 1968). The angular positions of the minima of the reflected beam are given by

$$\eta = \mp(K^2 \Lambda_B^2 t^{-2} + 1)^{1/2},$$

where K is an integer.

Integrated intensity. The integrated intensity is

$$I_{hi} = \pi\delta \tanh[\pi t/\Lambda_B], \qquad (5.1.7.8)$$

where t is the crystal thickness. When this thickness becomes very large, the integrated intensity tends towards

$$I_{hi} = \pi\delta. \qquad (5.1.7.9)$$

This expression differs from (5.1.7.3) by the factor π, which appears here in place of $8/3$. von Laue (1960) pointed out that because of the differences between the two expressions for the reflecting power, (5.1.7.2) and (5.1.7.7*b*), perfect agreement could not be expected. Since some absorption is always present, expression (5.1.7.3), which includes the factor $8/3$, should be used for very thick crystals. In the presence of absorption, however, expression (5.1.7.8) for the reflected intensity for thin crystals does tend towards that for thick crystals as the crystal thickness increases.

Comparison with geometrical theory. When t/Λ_B is very small (thin crystals or weak reflections), (5.1.7.8) tends towards

$$I_{hi} = R^2 \lambda^2 t |F_h|^2 / (V^2 \gamma_o \sin 2\theta), \qquad (5.1.7.10)$$

which is the expression given by geometrical theory. If we call this intensity I_{hi}(geom.), comparison of expressions (5.1.7.8) and (5.1.7.10) shows that the integrated intensity for crystals of intermediate thickness can be written

$$I_{hi} = I_{hi}(\text{geom.}) \frac{\tanh(\pi t/\Lambda_B)}{(\pi t/\Lambda_B)}, \qquad (5.1.7.11)$$

which is the expression given by Darwin (1922) for primary extinction.

5.1.7.2.2. *Absorbing crystals*

Reflected intensity. The intensity of the reflected wave for a thin absorbing crystal is

$$I_h = |\gamma| \left| \frac{D_h^{(a)}}{D_o^{(a)}} \right|^2 = \left| \frac{F_h}{F_{\bar{h}}} \right| \frac{\cosh 2b - \cos 2a}{L \cosh 2b + (L^2-1)^{1/2} \sinh 2b - \cos(2a + 2\Psi')}, \qquad (5.1.7.12)$$

where

$$2a = [\pi t/\Lambda_B] \rho \cos(\beta + \omega),$$
$$2b = [\pi t/\Lambda_B] \rho \sin(\beta + \omega).$$

L, ρ and ψ' are defined in (5.1.7.5), β is defined in (5.1.3.7) and ω is the phase angle of $(\eta^2 - 1)^{1/2}$.

Comparison with geometrical theory. When t/Λ_B decreases towards zero, expression (5.1.7.12) tends towards $[\sin(\pi t\eta/\Lambda_B)/\eta]^2$; using (5.1.3.5) and (5.1.3.8), it can be shown that expression (5.1.7.12) can be written, in the non-absorbing symmetric case, as

$$I_h = \frac{R^2\lambda^2C^2|F_h|^2t^2}{V^2\sin^2\theta}\left\{\frac{\sin[2\pi k\cos(\theta)t\Delta\theta]}{[2\pi k\cos(\theta)t\Delta\theta]}\right\}^2, \qquad (5.1.7.13)$$

where d is the lattice spacing and $\Delta\theta$ is the difference between the angle of incidence and the middle of the reflection domain. This expression is the classical expression given by geometrical theory [see, for instance, James (1950)].

5.1.8. Real waves

5.1.8.1. *Introduction*

The preceding sections have dealt with the diffraction of a plane wave by a semi-infinite perfect crystal. This situation is actually never encountered in practice, although with various devices, in particular using synchrotron radiation, it is possible to produce highly collimated monochromated waves which behave like pseudo plane waves. The wave from an X-ray tube is best represented by a spherical wave. The first experimental proof of this fact is due to Kato & Lang (1959) in the transmission case. Kato extended the dynamical theory to spherical waves for non-absorbing (1961*a*,*b*) and absorbing crystals (1968*a*,*b*). He expanded the incident spherical wave into plane waves by a Fourier transform, applied plane-wave dynamical theory to each of these components and took the Fourier transform of the result again in order to obtain the final solution. Another method for treating the problem was used by Takagi (1962, 1969), who solved the propagation equation in a medium where the lateral extension of the incident wave is limited and where the wave amplitudes depend on the lateral coordinates. He showed that in this case the set of fundamental linear equations (5.1.2.20) should be replaced by a set of partial differential equations. This treatment can be applied equally well to a perfect or to an imperfect crystal. In the case of a perfect crystal, Takagi showed that these equations have an analytical solution that is identical with Kato's result. Uragami (1969, 1970) observed the spherical wave in the Bragg (reflection) case, interpreting the observed intensity distribution using Takagi's theory. Saka *et al.* (1973) subsequently extended Kato's theory to the Bragg case.

Without using any mathematical treatment, it is possible to make some elementary remarks by considering the fact that the divergence of the incident beam falling on the crystal from the source is much larger than the angular width of the reflection domain. Fig. 5.1.8.1(*a*) shows a spatially collimated beam falling on a crystal in the transmission case and Fig. 5.1.8.1(*b*) represents the corresponding situation in reciprocal space. Since the divergence of the incident beam is larger than the angular width of the dispersion surface, the plane waves of its Fourier expansion will excite every point of both branches of the dispersion surface. The propagation directions of the corresponding wavefields will cover the angular range between those of the incident and reflected beams (Fig. 5.1.8.1*a*) and fill what is called the *Borrmann triangle.* The intensity distribution within this triangle has interesting properties, as described in the next two sections.

5.1.8.2. *Borrmann triangle*

The first property of the Borrmann triangle is that the angular density of the wavefield paths is inversely proportional to the curvature of the dispersion surface around their tie points. Let us consider an incident wavepacket of angular width $\delta(\Delta\theta)$. It will generate a packet of wavefields propagating within the Borrmann triangle. The angular width $\Delta\alpha$ (Fig. 5.1.8.2) between the paths of the corresponding wavefields is related to the radius of curvature $\mathcal{R}$ of the dispersion surface by

$$\mathcal{A} = \Delta\alpha/\delta(\Delta\theta) = k\cos\theta(\mathcal{R}\cos\alpha), \qquad (5.1.8.1)$$

where α is the angle between the wavefield path and the lattice planes [equation (5.1.2.26)] and $\mathcal{A}$ is called the amplification ratio. In the middle of the reflecting domain, the radius of curvature of the dispersion surface is very much shorter than its value, k, far from it (about 10^4 times shorter) and the amplification ratio is therefore very large. As a consequence, the energy of a wavepacket of width $\delta(\Delta\theta)$ in reciprocal space is spread in direct space over an angle $\Delta\alpha$ given by (5.1.8.1). The intensity distribution on the exit surface BC (Fig. 5.1.8.1*a*) is therefore proportional to $I_h/\mathcal{A}$. It is represented in Fig. 5.1.8.3 for several values of the absorption coefficient:

(i) Small values of $\mu_o t$ (less than 2 or 3) (Fig. 5.1.8.3*a*). The intensity distribution presents a wide minimum in the centre where the density of wavefields is small and increases very sharply at the edges where the density of wavefields is large, although it is the reverse for the reflecting power I_{hj}. This effect, called the *margin effect*, was predicted qualitatively by Borrmann (1959) and von Laue (1960), demonstrated experimentally by Kato & Lang (1959), and calculated by Kato (1960).

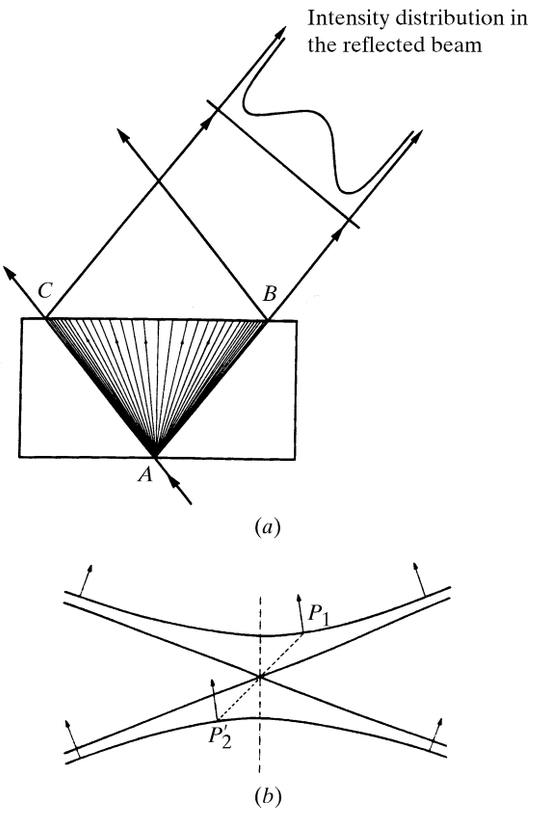

Fig. 5.1.8.1. Borrmann triangle. When the incident beam is divergent, the whole dispersion surface is excited and the wavefields excited inside the crystal propagate within a triangle filling all the space between the incident direction, AC, and the reflected direction, AB. Along any direction Ap within this triangle two wavefields propagate, having as tie points two conjugate points, P and P', at the extremities of a diameter of the dispersion surface. (*a*) Direct space; (*b*) reciprocal space.

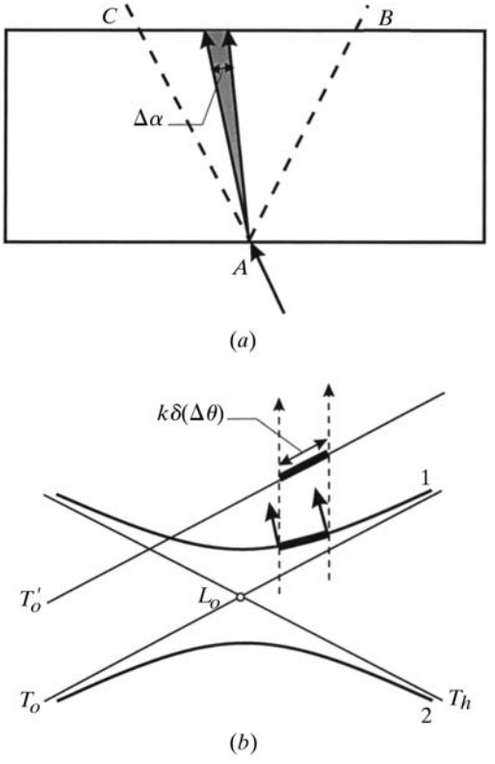

Fig. 5.1.8.2. Packet of wavefields of divergence $\Delta\alpha$ excited in the crystal by an incident wavepacket of angular width $\delta(\Delta\theta)$. (*a*) Direct space; (*b*) reciprocal space.

(ii) Large values of $\mu_o t$ (of the order of 6 or more) (Fig. 5.1.8.3*b*). The predominant factor is now anomalous absorption. The wavefields propagating along the edges of the Borrmann triangle undergo normal absorption, while those propagating parallel to the lattice planes (or nearly parallel) correspond to tie points in the centre of the dispersion surface and undergo anomalously low absorption. The intensity distribution now has a maximum in the centre. For values of μt larger than 10 or so, practically only the wavefields propagating parallel to the lattice planes go through the crystal, which acts as a wave guide: this is the Borrmann effect.

5.1.8.3. *Spherical-wave Pendellösung*

Fig. 5.1.8.4 shows that along any path *Ap* inside the Borrmann triangle two wavefields propagate, one with tie point P_1, on branch 1, the other with the point P_2', on branch 2. These two points lie on the extremities of a diameter of the dispersion surface. The two wavefields interfere, giving rise to *Pendellösung* fringes, which were first observed by Kato & Lang (1959), and calculated by Kato (1961*b*). These fringes are of course quite different from the plane-wave *Pendellösung* fringes predicted by Ewald (Section 5.1.6.3) because the tie points of the interfering wavefields are different and their period is also different, but they have in common the fact that they result from interference between wavefields belonging to different branches of the dispersion surface.

Kato has shown that the intensity distribution at any point at the base of the Borrmann triangle is proportional to

$$\left\{J_o\left[A(x_o x_h)^{1/2}\right]\right\}^2,$$

where $A = 2\pi(\gamma_o\gamma_h)^{1/2}/(\Lambda_L \sin\theta)$ and x_o and x_h are the distances of p from the sides AB and AC of the Borrmann triangle (Fig. 5.1.8.4). The equal-intensity fringes are therefore located along the locus of the points in the triangle for which the product of the distances to the sides is constant, that is hyperbolas having AB and AC as asymptotes (Fig. 5.1.8.4*b*). These fringes can be observed on a section topograph of a wedge-shaped crystal (Fig. 5.1.8.5). The technique of section topography is described in *IT* C, Section 2.7.2.2. The *Pendellösung* distance Λ_L depends on the polarization

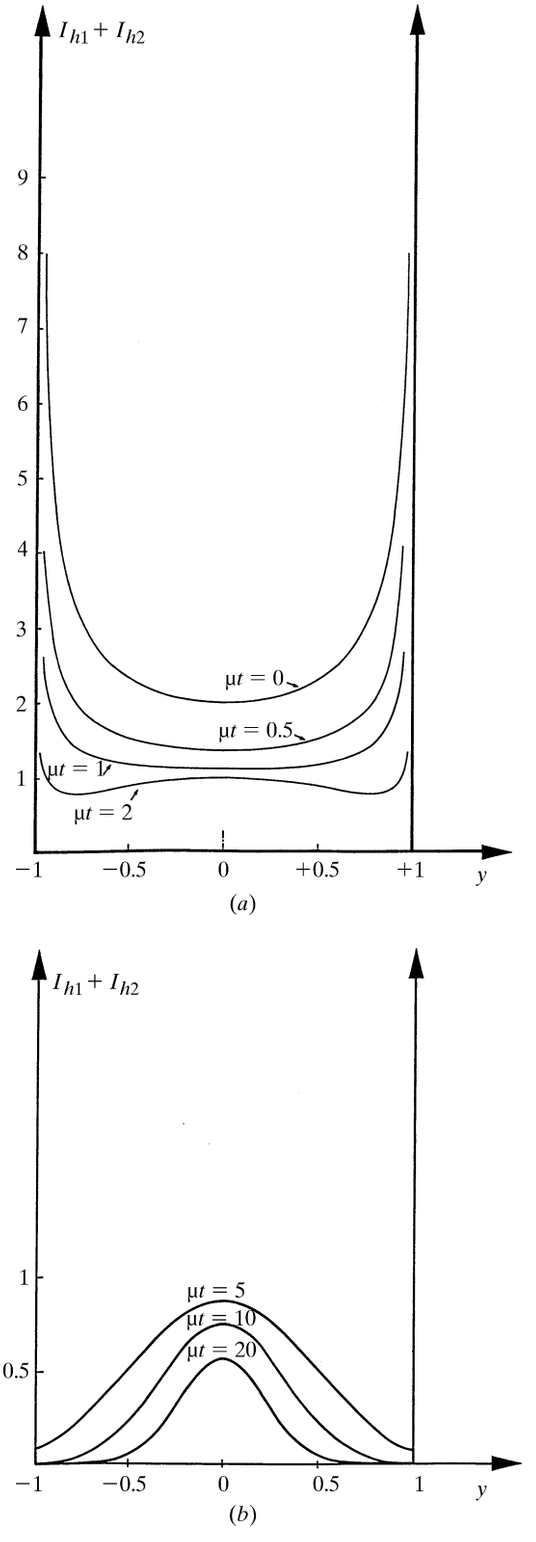

Fig. 5.1.8.3. Intensity distribution along the base of the Borrmann triangle. y is a normalized coordinate along BC. (*a*) Small values of μt. The interference (spherical-wave *Pendellösung*) between branch 1 and branch 2 is neglected. (*b*) Large values of μt.

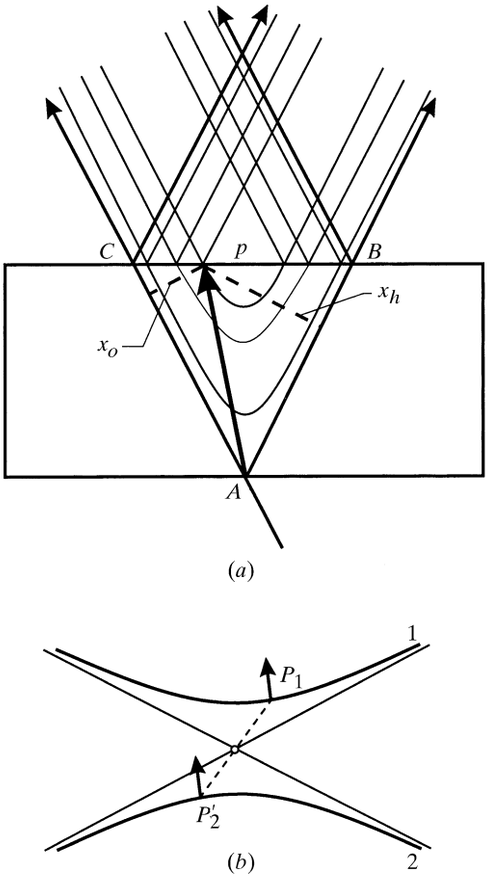

Fig. 5.1.8.4. Interference at the origin of the *Pendellösung* fringes in the case of an incident spherical wave. (*a*) Direct space; (*b*) reciprocal space.

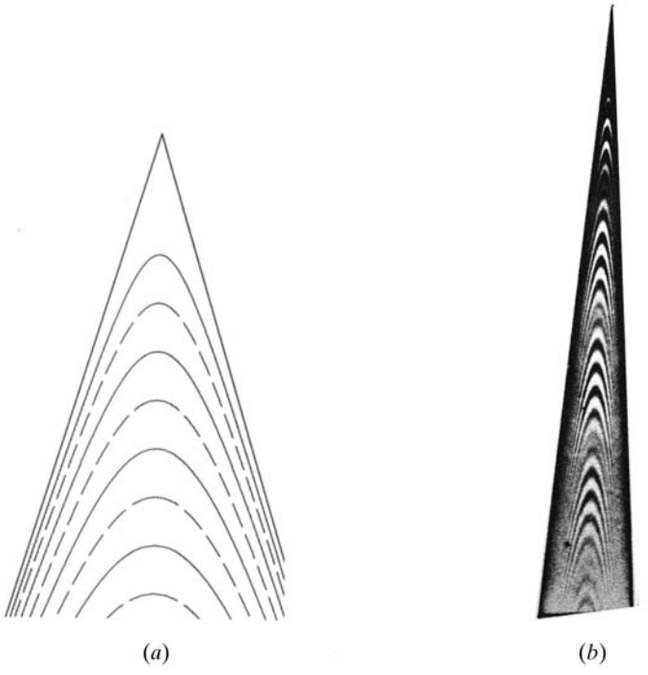

Fig. 5.1.8.5. Spherical-wave *Pendellösung* fringes observed on a wedge-shaped crystal. (*a*) Computer simulation (solid lines: maxima; dashed lines: minima). (*b*) X-ray section topograph of a wedge-shaped silicon crystal (444 reflection, Mo $K\alpha$ radiation).

state [see equation (5.1.3.8)]. If the incident wave is unpolarized, one observes the superposition of the *Pendellösung* fringes corresponding to the two states of polarization, parallel and perpendicular to the plane of incidence. This results in a beat effect, which is clearly visible in Fig. 5.1.8.5.

Appendix 5.1.1.

A5.1.1.1. *Dielectric susceptibility – classical derivation*

Under the influence of the incident electromagnetic radiation, the medium becomes polarized. The dielectric susceptibility, which relates this polarization to the electric field, thus characterizes the interaction of the medium and the electromagnetic wave. The classical derivation of the dielectric susceptibility, χ, which is summarized here is only valid for a very high frequency which is also far from an absorption edge. Let us consider an electromagnetic wave,

$$\mathbf{E} = \mathbf{E_o} \exp 2\pi i(\nu t - \mathbf{k}\cdot\mathbf{r}),$$

incident on a bound electron. The electron behaves as if it were held by a spring with a linear restoring force and is an oscillator with a resonant frequency ν_o. The equation of its motion is written in the following way:

$$m\, \mathrm{d}^2\mathbf{a}/\mathrm{d}t^2 = -4\pi^2\nu_o m\mathbf{a} = \mathbf{F},$$

where the driving force $\mathbf{F}$ is due to the electric field of the wave and is equal to $-e\mathbf{E}$. The magnetic interaction is neglected here.

The solution of the equation of motion is

$$\mathbf{a} = -e\mathbf{E}/[4\pi^2 m(\nu_o - \nu^2)].$$

The resonant frequencies of the electrons in atoms are of the order of the ultraviolet frequencies and are therefore much smaller than X-ray frequencies. They can be neglected and the expression of the amplitude of the electron reduces to

$$\mathbf{a} = e\mathbf{E}/(4\pi^2\nu^2).$$

The dipolar moment is therefore

$$\mathcal{M} = -e\mathbf{a} = -e^2\mathbf{E}/(4\pi^2\nu^2 m).$$

von Laue assumes that the negative charge is distributed continuously all over space and that the charge of a volume element $\mathrm{d}\tau$ is $-e\rho\ \mathrm{d}\tau$, where ρ is the electronic density. The electric moment of the volume element is

$$\mathrm{d}\mathcal{M} = -e^2\rho\mathbf{E}\ \mathrm{d}\tau/(4\pi^2\nu^2 m).$$

The polarization is equal to the moment per unit volume:

$$\mathbf{P} = \mathrm{d}\mathcal{M}/\mathrm{d}\tau = -e^2\rho\mathbf{E}/(4\pi^2\nu^2 m).$$

It is related to the electric field and electric displacement through

$$\mathbf{D} = \varepsilon_o\mathbf{E} + \mathbf{P} = \varepsilon_o(1+\chi)\mathbf{E}. \qquad \text{(A5.1.1.1)}$$

We finally obtain the expression of the dielectric susceptibility,

$$\chi = -e^2\rho/(4\pi^2\varepsilon_o\nu^2 m) = -R\lambda^2\rho/\pi, \qquad \text{(A5.1.1.2)}$$

where $R = e^2/(4\pi\varepsilon_o mc^2)$ $(= 2.81794 \times 10^{-15}$ m) is the classical radius of the electron.

A5.1.1.2. *Maxwell's equations*

The electromagnetic field is represented by two vectors, $\mathbf{E}$ and $\mathbf{B}$, which are the electric field and the magnetic induction, respectively. To describe the interaction of the field with matter, three other vectors must be taken into account, the electrical current density, $\mathbf{j}$, the electric displacement, $\mathbf{D}$, and the magnetic field, $\mathbf{H}$. The space and time derivatives of these vectors are related in a continuous

medium by Maxwell's equations:

$$\begin{aligned} \text{curl } \mathbf{E} &= -\partial\mathbf{B}/\partial t \\ \text{curl } \mathbf{H} &= \partial\mathbf{D}/\partial t + \mathbf{j} \\ \text{div } \mathbf{D} &= \rho \\ \text{div } \mathbf{B} &= 0, \end{aligned} \tag{A5.1.1.3}$$

where ρ is the electric charge density.

The electric field and the electric displacement on the one hand, and the magnetic field and the magnetic induction on the other hand, are related by the so-called *material relations*, which describe the reaction of the medium to the electromagnetic field:

$$\begin{aligned} \mathbf{D} &= \varepsilon\mathbf{E} \\ \mathbf{B} &= \mu\mathbf{H}, \end{aligned}$$

where ε and μ are the dielectric constant and the magnetic permeability, respectively.

These equations are complemented by the following boundary conditions at the surface between two neighbouring media:

$$\begin{aligned} \mathbf{E}_{T1} - \mathbf{E}_{T2} = 0 \quad \mathbf{D}_{N1} - \mathbf{D}_{N2} = 0 \\ \mathbf{H}_{T1} - \mathbf{H}_{T2} = 0 \quad \mathbf{B}_{N1} - \mathbf{B}_{N2} = 0. \end{aligned} \tag{A5.1.1.4}$$

From the second and the third equations of (A5.1.1.3), and using the identity

$$\text{div } (\text{curl } \mathbf{y}) = 0,$$

it follows that

$$\text{div } \mathbf{j} + \partial\rho/\partial t = 0. \tag{A5.1.1.5}$$

A5.1.1.3. *Propagation equation*

In a vacuum, ρ and $\mathbf{j}$ are equal to zero, and the first two equations of (A5.1.1.3) can be written

$$\begin{aligned} \text{curl } \mathbf{E} &= -\mu_0\partial\mathbf{E}/\partial t \\ \text{curl } \mathbf{H} &= \varepsilon_0\partial\mathbf{H}/\partial t, \end{aligned}$$

where ε_0 and μ_0 are the dielectric constant and the magnetic permeability of a vacuum, respectively.

By taking the curl of both sides of the second equation, it follows that

$$\text{curl curl } \mathbf{E} = -\varepsilon_0\mu_0\partial^2\mathbf{E}/\partial t^2.$$

Using the identity curl curl $\mathbf{E}$ = grad div $\mathbf{E} - \Delta\mathbf{E}$, the relation $\varepsilon_0\mu_0 = 1/c^2$, where c is the velocity of light, and noting that div $\mathbf{E}$ = div $\mathbf{D} = 0$, one finally obtains the equation of propagation of an electromagnetic wave in a vacuum:

$$\Delta\mathbf{E} = \frac{1}{c^2}\frac{\partial^2\mathbf{E}}{\partial t^2}. \tag{A5.1.1.6}$$

Its simplest solution is a plane wave:

$$\mathbf{E} = \mathbf{E_0}\exp 2\pi i(\nu t - \mathbf{k}\cdot\mathbf{r}),$$

of which the wavenumber $k = 1/\lambda$ and the frequency ν are related by

$$k = \nu/c.$$

The basic properties of the electromagnetic field are described, for instance, in Born & Wolf (1983).

The propagation equation of X-rays in a crystalline medium is derived following von Laue (1960). The interaction of X-rays with charged particles is inversely proportional to the mass of the particle and the interaction with the nuclei can be neglected. As a first approximation, it is also assumed that the magnetic interaction of X-rays with matter is neglected, and that the magnetic permeability μ can be taken as equal to the magnetic permeability of a vacuum, μ_0. It is further assumed that the negative and positive charges are both continuously distributed and compensate each other in such a way that there is neutrality and no current everywhere: ρ and $\mathbf{j}$ are equal to zero and div $\mathbf{D}$ is therefore also equal to zero. The electric displacement is related to the electric field by (A5.1.1.1) and the electric part of the interaction of X-rays with matter is expressed through the dielectric susceptibility χ, which is given by (A5.1.1.2). This quantity is proportional to the electron density and varies with the space coordinates. It is therefore concluded that div $\mathbf{E}$ is different from zero, as opposed to what happens in a vacuum. For this reason, the propagation equation of X-rays in a crystalline medium is expressed in terms of the electric displacement rather than in terms of the electric field. It is obtained by eliminating $\mathbf{H}$, $\mathbf{B}$ and $\mathbf{E}$ in Maxwell's equations and taking into account the above assumptions:

$$\Delta\mathbf{D} + \text{curl curl } \chi\mathbf{D} = \frac{1}{c^2}\frac{\partial^2\mathbf{E}}{\partial t^2}. \tag{A5.1.1.7}$$

Only coherent scattering is taken into account here, that is, scattering without frequency change. The solution is therefore a wave of the form

$$\mathbf{D}(\mathbf{r})\exp 2\pi i\nu t.$$

By replacing $\mathbf{D}$ with this expression in equation (A5.1.1.7), one finally obtains the propagation equation (5.1.2.2) (Section 5.1.2.1).

In a crystalline medium, χ is a triply periodic function of the space coordinates and the solutions of this equation are given in terms of Fourier series which can be interpreted as sums of electromagnetic plane waves. Each of these waves is characterized by its wavevector, $\mathbf{K_h}$, its electric displacement, $\mathbf{D_h}$, its electric field, $\mathbf{E_h}$, and its magnetic field, $\mathbf{H_h}$. It can be shown that, as a consequence of the fact that div $\mathbf{D} = 0$ and div $\mathbf{E} \neq 0$, $\mathbf{D_h}$ is a transverse wave ($\mathbf{D_h}$, $\mathbf{H_h}$ and $\mathbf{K_h}$ and are mutually orthogonal) while $\mathbf{E_h}$ is not. The electric displacement is therefore a more suitable vector for describing the state of the field inside the crystal than the electric field.

A5.1.1.4. *Poynting vector*

The propagation direction of the energy of an electromagnetic wave is given by that of the Poynting vector defined by (see Born & Wolf, 1983)

$$\mathbf{S} = \mathcal{R}(\mathbf{E}\wedge\mathbf{H}^*), \tag{A5.1.1.8}$$

where $\mathcal{R}()$ means real part of ().

The intensity I of the radiation is equal to the energy crossing unit area per second in the direction normal to that area. It is given by the value of the Poynting vector averaged over a period of time long compared with $1/\nu$:

$$\mathbf{I} = |\mathbf{S}| = c\varepsilon|\mathbf{E}|^2 = c|\mathbf{D}|^2/\varepsilon.$$

References

5.1

Authier, A. (1970). *Ewald waves in theory and experiment*. *Adv. Struct. Res. Diffr. Methods*, **3**, 1–51.

Authier, A. (1986). *Angular dependence of the absorption induced nodal plane shifts of X-ray stationary waves*. *Acta Cryst.* A**42**, 414–426.

Authier, A. (1989). *X-ray standing waves*. *J. Phys. (Paris)*, **50**, C7-215, C7-224.

Authier, A. (2001). *Dynamical theory of X-ray diffraction*. IUCr Monographs on Crystallography. Oxford University Press.

Authier, A. & Balibar, F. (1970). *Création de nouveaux champs d'onde généralisés dus à la présence d'un objet diffractant. II. Cas d'un défaut isolé*. *Acta Cryst.* A**26**, 647–654.

Authier, A. & Malgrange, C. (1998). *Diffraction physics*. *Acta Cryst.* A**54**, 806–819.

Batterman, B. W. (1964). *Effect of dynamical diffraction in X-ray fluorescence scattering*. *Phys. Rev. A*, **133**, 759–764.

Batterman, B. W. (1969). *Detection of foreign atom sites by their X-ray fluorescence scattering*. *Phys. Rev. Lett.* **22**, 703–705.

Batterman, B. W. & Bilderback, D. H. (1991). *X-ray monochromators and mirrors*. In *Handbook on synchrotron radiation*, Vol. 3, edited by G. Brown & D. E. Moncton, pp. 105–153. Amsterdam: Elsevier Science Publishers BV.

Batterman, B. W. & Cole, H. (1964). *Dynamical diffraction of X-rays by perfect crystals*. *Rev. Mod. Phys.* **36**, 681–717.

Batterman, B. W. & Hildebrandt, G. (1967). *Observation of X-ray Pendellösung fringes in Darwin reflection*. *Phys. Status Solidi*, **23**, K147–K149.

Batterman, B. W. & Hildebrandt, G. (1968). *X-ray Pendellösung fringes in Darwin reflection*. *Acta Cryst.* A**24**, 150–157.

Bedzyk, M. J. (1988). *New trends in X-ray standing waves*. *Nucl. Instrum. Methods A*, **266**, 679–683.

Bonse, U. & Teworte, R. (1980). *Measurement of X-ray scattering factors of Si from the fine structure of Laue case rocking curves*. *J. Appl. Cryst.* **13**, 410–416.

Born, M. & Wolf, E. (1983). *Principles of optics*, 6th ed. Oxford: Pergamon Press.

Borrmann, G. (1950). *Die Absorption von Röntgenstrahlen in Fall der Interferenz*. *Z. Phys.* **127**, 297–323.

Borrmann, G. (1954). *Der kleinste Absorption Koeffizient interfierender Röntgenstrahlung*. *Z. Kristallogr.* **106**, 109–121.

Borrmann, G. (1959). *Röntgenwellenfelder*. *Beit. Phys. Chem. 20 Jahrhunderts*, pp. 262–282. Braunschweig: Vieweg und Sohn.

Bragg, W. L. (1913). *The diffraction of short electromagnetic waves by a crystal*. *Proc. Cambridge Philos. Soc.* **17**, 43–57.

Bragg, W. L., Darwin, C. G. & James, R. W. (1926). *The intensity of reflection of X-rays by crystals*. *Philos. Mag.* **1**, 897–922.

Brümmer, O. & Stephanik, H. (1976). *Dynamische Interferenztheorie*. Leipzig: Akademische Verlagsgesellshaft.

Chang, S.-L. (1987). *Solution to the X-ray phase problem using multiple diffraction – a review*. *Crystallogr. Rev.* **1**, 87–189.

Cowan, P. L., Brennan, S., Jach, T., Bedzyk, M. J. & Materlik, G. (1986). *Observations of the diffraction of evanescent X-rays at a crystal surface*. *Phys. Rev. Lett.* **57**, 2399–2402.

Darwin, C. G. (1914*a*). *The theory of X-ray reflection*. *Philos. Mag.* **27**, 315–333.

Darwin, C. G. (1914*b*). *The theory of X-ray reflection*. *Part II. Philos. Mag.* **27**, 675–690.

Darwin, C. G. (1922). *The reflection of X-rays from imperfect crystals*. *Philos. Mag.* **43**, 800–829.

Ewald, P. P. (1917). *Zur Begründung der Kristalloptik. III. Röntgenstrahlen*. *Ann. Phys. (Leipzig)*, **54**, 519–597.

Ewald, P. P. (1958). *Group velocity and phase velocity in X-ray crystal optics*. *Acta Cryst.* **11**, 888–891.

Fewster, P. F. (1993). *X-ray diffraction from low-dimensional structures*. *Semicond. Sci. Technol.* **8**, 1915–1934.

Fingerland, A. (1971). *Some properties of the single crystal rocking curve in the Bragg case*. *Acta Cryst.* A**27**, 280–284.

Golovchenko, J. A., Patel, J. R., Kaplan, D. R., Cowan, P. L. & Bedzyk, M. J. (1982). *Solution to the surface registration problem using X-ray standing waves*. *Phys. Rev. Lett.* **49**, 560–563.

Hart, M. (1981). *Bragg angle measurement and mapping*. *J. Crystal Growth*, **55**, 409–427.

Hirsch, P. B. & Ramachandran, G. N. (1950). *Intensity of X-ray reflection from perfect and mosaic absorbing crystals*. *Acta Cryst.* **3**, 187–194.

Hümmer, K. & Weckert, E. (1995). *Enantiomorphism and three-beam X-ray diffraction: determination of the absolute structure*. *Acta Cryst.* A**51**, 431–438.

International Tables for Crystallography (1999). Vol. C. *Mathematical, physical and chemical tables*, edited by A. J. C. Wilson & E. Prince. Dordrecht: Kluwer Academic Publishers.

James, R. W. (1950). *The optical principles of the diffraction of X-rays*. London: G. Bell and Sons Ltd.

James, R. W. (1963). *The dynamical theory of X-ray diffraction*. *Solid State Phys.* **15**, 53.

Kato, N. (1955). *Integrated intensities of the diffracted and transmitted X-rays due to ideally perfect crystal*. *J. Phys. Soc. Jpn*, **10**, 46–55.

Kato, N. (1958). *The flow of X-rays and material waves in an ideally perfect single crystal*. *Acta Cryst.* **11**, 885–887.

Kato, N. (1960). *The energy flow of X-rays in an ideally perfect crystal: comparison between theory and experiments*. *Acta Cryst.* **13**, 349–356.

Kato, N. (1961*a*). *A theoretical study of Pendellösung fringes. Part I. General considerations*. *Acta Cryst.* **14**, 526–532.

Kato, N. (1961*b*). *A theoretical study of Pendellösung fringes. Part 2. Detailed discussion based upon a spherical wave theory*. *Acta Cryst.* **14**, 627–636.

Kato, N. (1963). *Pendellösung fringes in distorted crystals. I. Fermat's principle for Bloch waves*. *J. Phys. Soc. Jpn*, **18**, 1785–1791.

Kato, N. (1964*a*). *Pendellösung fringes in distorted crystals. II. Application to two-beam cases*. *J. Phys. Soc. Jpn*, **19**, 67–77.

Kato, N. (1964*b*). *Pendellösung fringes in distorted crystals. III. Application to homogeneously bent crystals*. *J. Phys. Soc. Jpn*, **19**, 971–985.

Kato, N. (1968*a*). *Spherical-wave theory of dynamical X-ray diffraction for absorbing perfect crystals. I. The crystal wave fields*. *J. Appl. Phys.* **39**, 2225–2230.

Kato, N. (1968*b*). *Spherical-wave theory of dynamical X-ray diffraction for absorbing perfect crystals. II. Integrated reflection power*. *J. Appl. Phys.* **39**, 2231–2237.

Kato, N. (1974). *X-ray diffraction*. In *X-ray diffraction*, edited by L. V. Azaroff, R. Kaplow, N. Kato, R. J. Weiss, A. J. C. Wilson & R. A. Young, pp. 176–438. New York: McGraw-Hill.

Kato, N. & Lang, A. R. (1959). *A study of Pendellösung fringes in X-ray diffraction*. *Acta Cryst.* **12**, 787–794.

Kikuta, S. (1971). *Determination of structure factors of X-rays using half-widths of the Bragg diffraction curves from perfect single crystals*. *Phys. Status Solidi B*, **45**, 333–341.

Kikuta, S. & Kohra, K. (1970). *X-ray collimators using successive asymmetric diffractions and their applications to measurements of diffraction curves. I. General considerations on collimators*. *J. Phys. Soc. Jpn*, **29**, 1322–1328.

Kovalchuk, M. V. & Kohn, V. G. (1986). *X-ray standing waves – a new method of studying the structure of crystals*. *Sov. Phys. Usp.* **29**, 426–446.

Laue, M. von (1931). *Die dynamische Theorie der Röntgenstrahlinterferenzen in neuer Form*. *Ergeb. Exakten Naturwiss.* **10**, 133–158.

Laue, M. von (1952). *Die Energie Strömung bei Röntgenstrahlinterferenzen Kristallen*. *Acta Cryst.* **5**, 619–625.

Laue, M. von (1960). *Röntgenstrahl-Interferenzen*. Frankfurt am Main: Akademische Verlagsgesellschaft.

5.1 (*cont.*)

Lefeld-Sosnowska, M. & Malgrange, C. (1968). *Observation of oscillations in rocking curves of the Laue reflected and refracted beams from thin Si single crystals*. *Phys. Status Solidi*, **30**, K23–K25.

Lefeld-Sosnowska, M. & Malgrange, C. (1969). *Experimental evidence of plane-wave rocking curve oscillations*. *Phys. Status Solidi*, **34**, 635–647.

Ludewig, J. (1969). *Debye–Waller factor and anomalous absorption (Ge; 293–5 K)*. *Acta Cryst.* A**25**, 116–118.

Materlik, G. & Zegenhagen, J. (1984). *X-ray standing wave analysis with synchrotron radiation applied for surface and bulk systems*. *Phys. Lett. A*, **104**, 47–50.

Ohtsuki, Y. H. (1964). *Temperature dependence of X-ray absorption by crystals. I. Photo-electric absorption*. *J. Phys. Soc. Jpn*, **19**, 2285–2292.

Ohtsuki, Y. H. (1965). *Temperature dependence of X-ray absorption by crystals. II. Direct phonon absorption*. *J. Phys. Soc. Jpn*, **20**, 374–380.

Penning, P. & Polder, D. (1961). *Anomalous transmission of X-rays in elastically deformed crystals*. *Philips Res. Rep.* **16**, 419–440.

Pinsker, Z. G. (1978). *Dynamical scattering of X-rays in crystals. Springer series in solid-state sciences*. Berlin: Springer-Verlag.

Prins, J. A. (1930). *Die Reflexion von Röntgenstrahlen an absorbierenden idealen Kristallen*. *Z. Phys.* **63**, 477–493.

Renninger, M. (1955). *Messungen zur Röntgenstrahl-Optik des Idealkristalls. I. Bestätigung der Darwin–Ewald–Prins–Kohler-Kurve*. *Acta Cryst.* **8**, 597–606.

Saka, T., Katagawa, T. & Kato, N. (1973). *The theory of X-ray crystal diffraction for finite polyhedral crystals. III. The Bragg–(Bragg)^m cases*. *Acta Cryst.* A**29**, 192–200.

Takagi, S. (1962). *Dynamical theory of diffraction applicable to crystals with any kind of small distortion*. *Acta Cryst.* **15**, 1311–1312.

Takagi, S. (1969). *A dynamical theory of diffraction for a distorted crystal*. *J. Phys. Soc. Jpn*, **26**, 1239–1253.

Tanner, B. K. (1976). *X-ray diffraction topography*. Oxford: Pergamon Press.

Tanner, B. K. (1990). *High resolution X-ray diffraction and topography for crystal characterization*. *J. Cryst. Growth*, **99**, 1315–1323.

Tanner, B. K. & Bowen, D. K. (1992). *Synchrotron X-radiation topography*. *Mater. Sci. Rep.* **8**, 369–407.

Uragami, T. (1969). *Pendellösung fringes of X-rays in Bragg case*. *J. Phys. Soc. Jpn*, **27**, 147–154.

Uragami, T. (1970). *Pendellösung fringes in a crystal of finite thickness*. *J. Phys. Soc. Jpn*, **28**, 1508–1527.

Wagner, E. H. (1959). *Group velocity and energy (or particle) flow density of waves in a periodic medium*. *Acta Cryst.* **12**, 345–346.

Zachariasen, W. H. (1945). *Theory of X-ray diffraction in crystals*. New York: John Wiley.

Zegenhagen, J. (1993). *Surface structure determination with X-ray standing waves*. *Surf. Sci. Rep.* **18**, 199–271.

5.2

Berry, M. V. (1971). *Diffraction in crystals at high voltages*. *J. Phys. C*, **4**, 697–722.

Bethe, H. A. (1928). *Theorie der Beugung von Elektronen an Kristallen*. *Ann. Phys. (Leipzig)*, **87**, 55–129.

Blackman, M. (1939). *Intensities of electron diffraction rings*. *Proc. Phys. Soc. London Sect. A*, **173**, 68–72.

Blume, J. (1966). *Die Kantenstreifung im Elektronen-Mikroskopischen Bild Wurfelformiger MgO Kristalle bei Durchstrahlung im Richtung der Raumdiagonal*. *Z. Phys.* **191**, 248–272.

Born, M. (1926). *Quantenmechanik der Stossvorgange*. *Z. Phys.* **38**, 803–826.

Buxton, B. (1978). *Graduate lecture-course notes: dynamical diffraction theory*. Cambridge University, England.

Corones, J., De Facio, B. & Kreuger, R. J. (1982). *Parabolic approximations to the time-independent elastic wave equation*. *J. Math. Phys.* **23**, 577–586.

Cowley, J. M. (1981). *Diffraction physics*, pp. 26–30. Amsterdam: North-Holland.

Cowley, J. M. & Moodie, A. F. (1957). *The scattering of electrons by atoms and crystals. I. A new theoretical approach*. *Acta Cryst.* **10**, 609–619.

Cowley, J. M. & Moodie, A. F. (1962). *The scattering of electrons by thin crystals*. *J. Phys. Soc. Jpn*, **17**, Suppl. B11, 86–91.

Feynman, R. (1948). *Space–time approach to non-relativistic quantum mechanics*. *Rev. Mod. Phys.* **201**, 367–387.

Frazer, R. A., Duncan, W. J. & Collar, A. R. (1963). *Elementary matrices*, pp. 78–79. Cambridge University Press.

Fujimoto, F. (1959). *Dynamical theory of electron diffraction in the Laue case*. *J. Phys. Soc. Jpn*, **14**, 1558–1568.

Fujiwara, K. (1959). *Application of higher order Born approximation to multiple elastic scattering of electrons by crystals*. *J. Phys. Soc. Jpn*, **14**, 1513–1524.

Fujiwara, K. (1962). *Relativistic dynamical theory of electron diffraction*. *J. Phys. Soc. Jpn*, **17**, Suppl. B11, 118–123.

Fukuhara, A. (1966). *Many-ray approximations in the dynamical theory of electron diffraction*. *J. Phys. Soc. Jpn*, **21**, 2645–2662.

Gilmore, R. (1974). *Lie groups, Lie algebras, and some of their applications*. New York: Wiley–Interscience.

Gjønnes, J. & Høier, R. (1971). *The application of non-systematic many-beam dynamic effects to structure-factor determination*. *Acta Cryst.* A**27**, 313–316.

Gjønnes, J. & Moodie, A. F. (1965). *Extinction conditions in the dynamic theory of electron diffraction*. *Acta Cryst.* **19**, 65–67.

Goodman, P. (1975). *A practical method of three-dimensional space-group analysis using convergent-beam electron diffraction*. *Acta Cryst.* A**31**, 804–810.

Goodman, P. (1981). Editor. *Fifty years of electron diffraction*. Dordrecht: Kluwer Academic Publishers.

Goodman, P. & Moodie, A. F. (1974). *Numerical evaluation of N-beam wave functions in electron scattering by the multislice method*. *Acta Cryst.* A**30**, 280–290.

Gratias, D. & Portier, R. (1983). *Time-like perturbation method in high energy electron diffraction*. *Acta Cryst.* A**39**, 576–584.

Hirsch, P. B., Howie, A., Nicholson, R. B., Pashley, D. W. & Whelan, M. J. (1965). *Electron microscopy of thin crystals*. London: Butterworths.

Howie, A. (1966). *Diffraction channelling of fast electrons and positrons in crystals*. *Philos. Mag.* **14**, 223–237.

Howie, A. (1978). In *Electron diffraction 1927–1977*, edited by P. J. Dobson, J. B. Pendry & C. J. Humphreys, pp. 1–12. *Inst. Phys. Conf. Ser.* No. 41. Bristol/London: Institute of Physics.

Humphreys, C. J. (1979). *The scattering of fast electrons by crystals*. *Rep. Prog. Phys.* **42**, 1825–1887.

Hurley, A. C., Johnson, A. W. S., Moodie, A. F., Rez, P. & Sellar, J. R. (1978). *Algebraic approaches to N-beam theory*. In *Electron diffraction 1927–1977*, edited by P. J. Dobson, J. B. Pendry & C. J. Humphreys, pp. 34–40. *Inst. Phys. Conf. Ser.* No. 41. Bristol/London: Institute of Physics.

Hurley, A. C. & Moodie, A. F. (1980). *The inversion of the three-beam intensities for scalar scattering by a general centrosymmetric crystal*. *Acta Cryst.* A**36**, 737–738.

International Tables for Crystallography (1999). Vol. C. *Mathematical, physical and chemical tables*, edited by A. J. C. Wilson & E. Prince. Dordrecht: Kluwer Academic Publishers.

Kainuma, Y. (1968). *Averaged intensities in the many beam dynamical theory of electron diffraction. Part I*. *J. Phys. Soc. Jpn*, **25**, 498–510.

Kambe, K. (1957). *Study of simultaneous reflection in electron diffraction by crystal*. *J. Phys. Soc. Jpn*, **12**, 13–31.

Kogiso, M. & Takahashi, H. (1977). *Group-theoretical method in the many-beam theory of electron diffraction*. *J. Phys. Soc. Jpn*, **42**, 223–229.

Lontovitch, M. & Fock, R. (1946). *Solution of the problem of propagation of electromagnetic waves along the Earth's surface by the method of parabolic equation*. *J. Phys.* **10**, 13–24. (Translated from Russian by J. Smorodinsky.)

Lynch, D. F. & Moodie, A. F. (1972). *Numerical evaluation of low energy electron diffraction intensities*. *Surf. Sci.* **32**, 422–438.